

# JGR Solid Earth

## RESEARCH ARTICLE

10.1029/2022JB026083

### Key Points:

- The Zn isotopic variations (0.04‰–0.46‰) of the clinopyroxenites are produced by melt metasomatism
- The “glassy” xenolith may represent the preserved sediment melt with recycled carbonate-bearing terrigenous components
- Zn isotopes can be used to trace the activity of slab-derived sediment melts in the sub-continental lithosphere

### Supporting Information:

Supporting Information may be found in the online version of this article.

### Correspondence to:

Y. Liu,  
[yshliu@cug.edu.cn](mailto:yshliu@cug.edu.cn)

### Citation:

Zhang, G., Liu, Y., Xu, R., Moynier, F., Zhu, Y., Ren, H., et al. (2023). Tracing sediment melt activity in the sub-continental lithosphere: Insights from Zn-Fe stable isotopes. *Journal of Geophysical Research: Solid Earth*, 128, e2022JB026083. <https://doi.org/10.1029/2022JB026083>

Received 21 NOV 2022

Accepted 12 APR 2023

### Author Contributions:

**Conceptualization:** Ganglan Zhang

**Data curation:** Ganglan Zhang, Yongsheng Liu

**Funding acquisition:** Yongsheng Liu

**Investigation:** Ganglan Zhang, Yongsheng Liu

**Methodology:** Yangtao Zhu, Xin Jiang, Ming Li




**Supervision:** Yongsheng Liu

**Visualization:** Ganglan Zhang

**Writing – original draft:** Ganglan Zhang, Frédéric Moynier

**Writing – review & editing:** Ganglan Zhang, Yongsheng Liu, Rong Xu, Frédéric Moynier, Yangtao Zhu, Huang Ren

## Tracing Sediment Melt Activity in the Sub-Continental Lithosphere: Insights From Zn-Fe Stable Isotopes

Ganglan Zhang<sup>1,2</sup> , Yongsheng Liu<sup>2</sup> , Rong Xu<sup>3</sup>, Frédéric Moynier<sup>4</sup> , Yangtao Zhu<sup>2</sup>, Huang Ren<sup>2</sup>, Xin Jiang<sup>2</sup>, and Ming Li<sup>2</sup>

<sup>1</sup>Key Laboratory of Marine Mineral Resources, Ministry of Natural Resources, Guangzhou Marine Geological Survey, China Geological Survey, Guangzhou, China, <sup>2</sup>State Key Laboratory of Geological Processes and Mineral Resources, School of Earth Sciences, China University of Geosciences, Wuhan, China, <sup>3</sup>State Key Laboratory of Ore Deposit Geochemistry, Institute of Geochemistry, Chinese Academy of Sciences, Guiyang, China, <sup>4</sup>Université Paris Cité, Institut de Physique du Globe de Paris, CNRS UMR 7154, Paris Cedex 05, France

**Abstract** Recycling of upper crustal sediments through slab subduction contributes to sub-continental lithospheric refertilization and heterogeneity. However, the nature of recycled upper crustal components is unclear and direct evidence for sediment melt activity in the sub-continental lithosphere is lacking. Here, we integrate major and trace elements, zircon U-Pb dating, Sr-Nd-Zn-Fe isotopic compositions of clinopyroxenites (crust-mantle boundary) and a “glassy” xenolith from the North China Craton to relate their petrogenesis to the potential recycling of upper continental crust and provide direct insight into the sediment melt-rock interaction. The clinopyroxenites have relatively uniform  $\delta^{56}\text{Fe}$  values (the permil deviation of the  $^{56}\text{Fe}/^{54}\text{Fe}$  ratio from the IRMM014;  $-0.05\text{‰}$ – $0.07\text{‰}$ , except for one outlier) and are not affected by melt metasomatism. The clinopyroxenites have highly variable whole-rock  $\delta^{66}\text{Zn}$  values (the permil deviation of the  $^{66}\text{Zn}/^{64}\text{Zn}$  ratio from the JMC-Lyon standard) between 0.04‰ and 0.46‰, that closely correlate with Rb/La, K/U, Ba/Th, and Th/Nb ratios, and generate arrays that trend toward a composition similar to the “glassy” xenolith. The “glassy” xenolith has a high  $\delta^{66}\text{Zn}$  value ( $0.43\text{‰} \pm 0.05\text{‰}$ , 2SD) and a significantly low  $^{143}\text{Nd}/^{144}\text{Nd}$  ratio (0.510991). This evidence implies that the “glassy” xenolith may represent a quenched sediment melt formed by the melting of carbonate-bearing terrigenous sediments that may also be responsible for the metasomatism of clinopyroxenite xenoliths. The geochemical evidence from the “glassy” and clinopyroxenite xenoliths provides a direct evidence for the activity of sediment melt with upper continental crust components in the sub-continental lithosphere.

**Plain Language Summary** Slab-derived sediment melt activity in the overlying lithosphere is crucial for element cycling and lithospheric evolution. To understand the nature of recycled sediment and its impact on the overlying lithosphere, we analyzed the Zn-Fe-Sr-Nd isotopic compositions of clinopyroxenites and a “glassy” xenolith from the North China Craton. The  $\delta^{66}\text{Zn}$  values of clinopyroxenites show correlations with proxies for hydrous melt metasomatism (Rb/La, K/U, Ba/Th, and Th/Nb ratios) and generate arrays that trend toward a composition similar to the “glassy” xenolith. The identification of “glassy” xenolith provides direct insight into the sediment melt-rock interaction. Furthermore, this study proves the validity of using Zn isotopes as a powerful tool for tracing sediment melt activity in the sub-continental lithosphere.

## 1. Introduction

The Earth's surface is shaped by plate tectonics through the cycle of continental amalgamation and breakup (Hawkesworth et al., 2020). Slab subduction at convergent margins triggered by plate tectonics would promote mass transfer between the Earth's surface and interior (e.g., Plank & Langmuir, 1998). Fluids and melts released from sediments, altered oceanic crust, and serpentinites in subducted slab could metasomatize the overlying lithosphere and modify its physical and chemical properties (e.g., oxidation state; Evans et al., 2012; G. Zhang et al., 2022). Therefore, tracing the nature of slab-derived sediment melts/fluids and their activities in the overlying lithosphere (mantle and mantle-crust boundary) are essential for understanding element cycles and lithospheric evolution. Hereto, the recycled signature of upper continental crust recorded by the overlying lithosphere, however, is extremely limited, and the nature of recycled upper crustal components and their impact on the overlying lithosphere remain poorly constrained.

Zinc and Fe isotopes have been used to trace the nature of slab-derived melts/fluids and element mobility in subduction zones (e.g., Z. Chen et al., 2021; Debret et al., 2016, 2021; Foden et al., 2018; S.-A. Liu et al., 2016; Nebel et al., 2015; Pons et al., 2016; R. Xu et al., 2022). For example, Debret et al. (2016) and Pons et al. (2016) observed that serpentinites are getting progressively enriched in the heavier isotopes of Fe and depleted in the lighter isotopes of Zn with the subduction-related metamorphic grade, respectively. These variations were interpreted as the lighter Fe and heavier Zn isotopes were preferentially released into the fluids during serpentine devolatilization (Debret et al., 2016; Pons et al., 2016). Also, the Kohistan gem olivine metasomatized by slab-derived fluids displays low  $\delta^{56}\text{Fe}$  ( $-0.36\text{‰}$ – $-0.06\text{‰}$ ) and high  $\delta^{66}\text{Zn}$  ( $0.57\text{‰}$ – $0.89\text{‰}$ ) values relative to that of mantle olivine ( $\delta^{56}\text{Fe}$ :  $\sim 0\text{‰}$ ;  $\delta^{66}\text{Zn}$ :  $\sim 0.18\text{‰}$ ) (Debret et al., 2018; Pons et al., 2016). Furthermore, the heavier Zn isotopic compositions of chlorite-bearing harzburgite from the Cerro del Almiraz massif were interpreted as the results of metasomatism by carbonate-bearing fluids derived from slab metasediments (Debret et al., 2021). However, the lack of arc lavas with high  $\delta^{66}\text{Zn}$  values (Huang et al., 2018) indicates that the heavy Zn isotopic signatures of slab-derived fluids/melts may be diluted by a much larger proportion of isotopically unfractionated Zn in the mantle wedge. Furthermore, the cause of the light Fe isotopic compositions in arc lavas, whether it is due to melt extraction or the addition of slab-derived melts/fluids, is still a matter of debate (e.g., Deng et al., 2022; Foden et al., 2018). Therefore, it is challenging to constrain the influence of the slab-derived melts/fluids on the Zn-Fe isotopic compositions of the overlying lithosphere from the perspective of arc volcanic lavas. The sub-continental lithosphere overlying subducted slab is the main sink for various slab-derived melts/fluids. Therefore, to explore the potential of Zn-Fe isotopes in tracking the nature of melts released from slab sediments and identifying their activities within subduction-influenced lithosphere, systematic studies on overlying lithospheric pyroxenites or peridotites metasomatized by sediment melts are required.

Previously reported Zn-Fe isotopic compositions of metasomatized pyroxenites and peridotites generally reflect kinetic isotopic fractionation during melt metasomatism (e.g., Huang et al., 2019; Wang et al., 2017; X. Zhao et al., 2017). Therefore, these studies could not determine the nature of metasomatic melts and provide direct evidence for melt-rock reactions. The clinopyroxenite xenoliths (crust-mantle boundary) carried by the Neogene Hannuoba basalts from the northern margin of North China Craton (NCC) provide an opportunity to study the potential of Zn-Fe isotopes in tracing the activity of slab-derived sediment melts in the sub-continental lithosphere. Previous studies suggested that the formation of the Hannuoba clinopyroxenites involved enriched recycled crustal components (sedimentary carbonates and upper crustal materials) (J. Hu et al., 2019; Y. Hu et al., 2016; Y. Xu, 2002; X. Zhao et al., 2017; Zheng et al., 2009). In this study, we combine new chemical and Sr-Nd isotopic data with published data on the Hannuoba clinopyroxenite xenoliths. Additionally, the Zn-Fe stable isotopic ratios of a “glassy” xenolith (mainly composed of quenched glass) and clinopyroxenites (whole-rock samples and mineral separates) were analyzed. The Zn-Fe isotopic studies of clinopyroxenites show that the inter-mineral Zn-Fe isotopic fractionation has reached equilibrium. Therefore, the Zn-Fe isotopic compositions of these whole-rock samples and mineral separates allow us to trace the recycling process of subducted sediment and sediment melt activity in the sub-continental lithosphere.

## 2. Geological Setting and Samples

The NCC is among the oldest continental blocks globally, dating back to 3.8 Ga. During the late Paleoproterozoic, the Eastern and Western Block were united along the intervening Trans-North China Orogen, resulting in the final cratonization of NCC (G. Zhao et al., 2001). Slab subduction since the Paleozoic has triggered extensive tectonothermal reactivation in the NCC, resulting in the formation of sizable granitic intrusions, volcanic eruptions, and metamorphic core complexes (Wu et al., 2019 and references therein). The lithospheric evolution of the NCC's northern margin has been strongly influenced by the southward subduction of the Paleo-Asian Ocean Plate, which is reflected in the widespread distribution of Carboniferous to Triassic intrusive suites (S.-H. Zhang et al., 2009). Also, enriched elemental and radiogenic isotopic compositions of the mantle peridotites and pyroxenites indicate crustal components (sediments and altered oceanic crust) from the Paleo-Asian Ocean Plate have been transported into the lithospheric mantle (e.g., Y. Liu et al., 2010; Y. Xu, 2002). The Neogene Hannuoba basalts on the NCC's northern margin consist of alternating layers of tholeiitic and alkaline basalts and have captured abundant deep-seated xenoliths, including peridotites, pyroxenites, granulites, and metasediments (Y. Liu et al., 2005, 2010; Zhi et al., 1990).

This study collected 11 clinopyroxenites and a “glassy” xenolith from the Hannuoba basalts. These xenoliths are typically spherical or ellipsoidal and range in diameters from 4 to 10 cm, exhibit protogranular texture and have

coarse to medium mineral grain sizes (0.5–5 mm) (Figures 1a and 1b). They are mainly composed of clinopyroxene (Cpx, diopside, more than 90 vol%) and are free of olivine (Ol) and orthopyroxene (Opx) (Figure 1). Phlogopite (Phl, <10 vol%) is present in some clinopyroxenites as an interstitial phase (Figure 1b). Spinel (Sp, <1 vol%) is only present in sample DMP138. Also, some accessory minerals (e.g., apatite and zircon) are identified under a binocular microscope (Figure S1 in Supporting Information S1). Petrographic observations show that no apparent superficial alteration has occurred in these clinopyroxenites. For the purposes of this study, samples with and without phlogopite are collectively referred to as phl-clinopyroxenite and pure-clinopyroxenite, respectively.

The hand specimen of the “glassy” xenolith (DMP528) is dark green and displays a clear boundary with the black host basalts (Figures 1c and 1d). Thin-section photomicrographs show that this xenolith is mainly composed of quenched glass with only a small number (<2 vol%) of minerals (e.g., apatite, carbonate, Fe-oxides, orthopyroxene) (Figures 1e–1h; Figure S2 in Supporting Information S1). The carbonate, Fe-oxides, and orthopyroxene exhibit partially resorbed textures and are fragmented into many micro-grains (Figures S2b–S2d in Supporting Information S1). Additionally, a large number of minute nucleated microlites and globulites appear in the glassy matrix of this xenolith (Figures 1e–1h). To evaluate the petrogenesis of the Hannuoba clinopyroxenites, six Al-augite websterites (Al-websterites) xenoliths from the Hannuoba basalts were also analyzed for comparison. These Al-websterites are characterized by medium mineral grain size (~1 mm) and irregular mineral boundaries. They consist of orthopyroxene (15–55 vol%) and clinopyroxene (45–85 vol%).

### 3. Analytical Methods

Zinc and Fe isotopic analyses were conducted at the State Key Laboratory of Geological Processes and Mineral Resources at China University of Geoscience (Wuhan), utilizing established protocols by Lei et al. (2022) and Zhu et al. (2019). Clinopyroxene, phlogopite, and spinel grains from the clinopyroxenites were handpicked under a binocular microscope. Whole-rock powders and pre-cleaned mineral fragments were dissolved using double-distilled concentrated HF and HNO<sub>3</sub>. Pre-cleaned AG-MP-1M anion resin was utilized to achieve separation of Zn and Fe.

Zinc and Fe isotope ratios were measured using a Nu Plasma 1,700 multi-collector inductively-coupled-plasma mass-spectrometry (MC-ICP-MS) and are reported in standard  $\delta$ -notation in permil relative to JMC Lyon 3-0749L and IRMM014, respectively. The measured  $\delta^{66}\text{Zn}$  and  $\delta^{56}\text{Fe}$  values of reference standards (BHVO-2, BIR-1, and W-2) in this study agree with recommended values within uncertainty (He et al., 2015; Moynier et al., 2017; Sossi et al., 2015) (Table 1). Furthermore, the replicate analyses of samples yielded identical  $\delta^{66}\text{Zn}$  and  $\delta^{56}\text{Fe}$  values within the long-term reproducibility (0.05‰) (Table 1), indicating the high precision and accuracy of the analytical method employed.

Detailed descriptions of the analytical methods used for the major and trace element contents of whole-rock and minerals, zircon U-Pb dating, Sr-Nd isotopic analyses of whole-rock, and clinopyroxene can be found in the Supplementary Materials.

## 4. Results

### 4.1. Major and Trace Element Compositions

#### 4.1.1. Whole-Rock

The major and trace element compositions of clinopyroxenites, Al-websterites, and the “glassy” xenolith are provided in Table S1 in Supporting Information S1. Clinopyroxenites have higher Mg# ( $=\text{Mg}/(\text{Mg} + \text{Fe}) \times 100$ , atomic number; 83.2–92.6), CaO (18.1–22.1 wt.%), and K<sub>2</sub>O (0.01–0.79 wt.%), but lower MgO (12.5–16.1 wt.%), total FeO (FeO<sub>T</sub>, 2.28–5.13 wt.%), Ni (14.9–34.5 ppm), and Cr (8.26–71.9 ppm) contents than those of the Al-websterites (Figure 2). Clinopyroxenites show convex-upward rare earth element (REE) patterns coupled with slightly negative Eu anomalies ( $\text{Eu}/\text{Eu}^* = 0.52\text{--}0.92$ , in which  $\text{Eu}/\text{Eu}^*$  is defined as  $2\text{Eu}_N/(\text{Sm}_N + \text{Gd}_N)$ , where the subscript N indicates normalization to chondritic values from McDonough and Sun (1995)) (Figures 3a and 3c). The phl-clinopyroxenites have significantly higher Rb and Ba contents than that of pure-clinopyroxenites (Figures 3b and 3d).

Sample DMP528 has high MgO (21.29 wt.%) and Al<sub>2</sub>O<sub>3</sub> (16.21 wt.%) but low FeO<sub>T</sub> (1.79 wt.%), Cr (18.3 ppm), and Ni (12.6 ppm) contents (Figure 2). It is characterized by enrichments in Rb, Ba and Pb, and displays light-REE (LREE)-enriched patterns in the primitive mantle (PM)-normalized diagrams (Figures 3e and 3f).

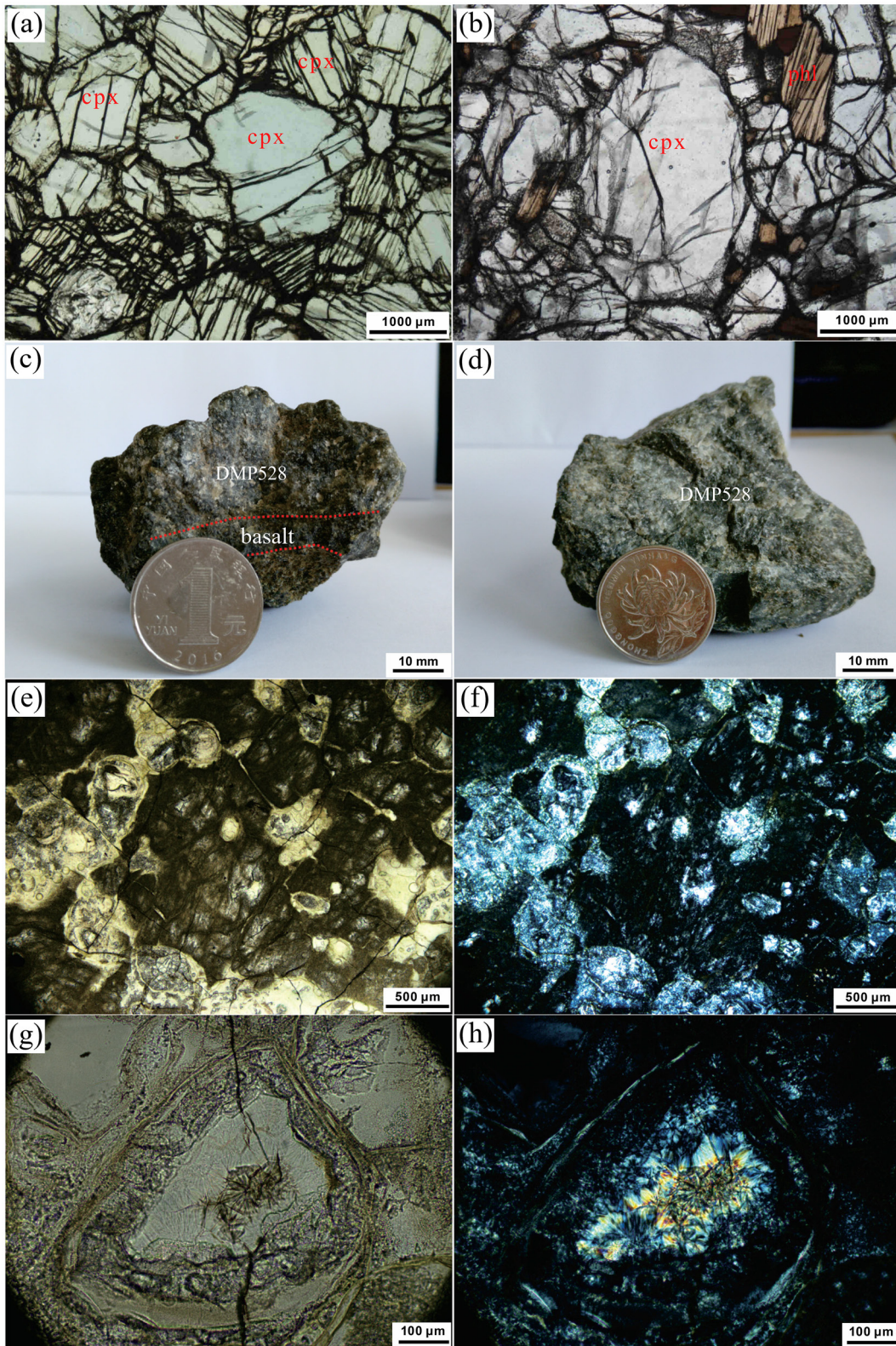


**Figure 1.** Hand specimen photographs and thin-section photomicrographs of representative textures in the Hannuoba clinopyroxenites and sample DMP528. (a) Medium-coarse grained texture of the pure-clinopyroxenite (DMP335); (b) clinopyroxene and phlogopite in the phl-clinopyroxenite (DMP392); (c, d) hand specimen photographs of sample DMP528, which displays a clear boundary with the host basalts; (e, f) abundantly nucleated microlites in sample DMP528 under plane- and cross-polarized light; (g, h) globulites in sample DMP528 under plane- and cross-polarized light. Cpx, clinopyroxene; Phl, phlogopite.

**Table 1**  
*Zinc-Fe Isotopic Compositions of Bulk-Rock and Mineral Separates of the Studies Samples and Reference Materials*

Sample	Lithology		$\delta^{66}\text{Zn}$ (‰)	2SD	$\delta^{68}\text{Zn}$ (‰)	2SD	<i>N</i>	$\delta^{56}\text{Fe}$ (‰)	2SD	$\delta^{57}\text{Fe}$ (‰)	2SD	<i>N</i>
DMP138	Phl-clinopyroxenite	Bulk rock	0.23	0.05	0.45	0.08	3	0.07	0.05	0.09	0.08	3
DMP13	Phl-clinopyroxenite	Bulk rock	0.45	0.05	0.81	0.08	3	0.04	0.05	0.09	0.08	3
		Phlogopite	0.46	0.05	0.95	0.08	3	0.05	0.05	0.07	0.08	3
		Clinopyroxene	0.48	0.05	1.04	0.08	3	0.10	0.05	0.11	0.08	3
DMP392	Phl-clinopyroxenite	Bulk rock	0.46	0.05	0.87	0.08	3	0.07	0.05	0.10	0.08	3
		Phlogopite	0.49	0.05	1.05	0.08	3	0.12	0.05	0.14	0.08	3
		Clinopyroxene	0.50	0.05	1.03	0.08	3	0.13	0.05	0.19	0.08	3
DMP107	Phl-clinopyroxenite	Bulk rock	0.28	0.05	0.57	0.08	3	-0.06	0.05	-0.09	0.08	3
		Phlogopite						-0.06	0.05	-0.12	0.08	3
		Clinopyroxene						-0.06	0.05	-0.13	0.08	3
		Spinel						-0.02	0.05	-0.05	0.08	3
DMP333	Pure-clinopyroxenite	Bulk rock	0.09	0.05	0.22	0.08	3	-0.03	0.05	-0.05	0.08	3
		Clinopyroxene	0.09	0.05	0.20	0.08	3	-0.07	0.05	-0.10	0.08	3
DMP335	Pure-clinopyroxenite	Bulk rock	0.24	0.05	0.52	0.08	3	0.04	0.05	0.07	0.08	3
		Clinopyroxene	0.28	0.05	0.60	0.08	3	0.04	0.05	0.07	0.08	3
DMP129	Pure-clinopyroxenite	Bulk rock	0.12	0.05	0.28	0.08	3	0.01	0.05	0.00	0.08	3
		Clinopyroxene	0.11	0.05	0.27	0.08	3	-0.01	0.05	-0.01	0.08	3
DMP340	Pure-clinopyroxenite	Bulk rock	0.21	0.05	0.43	0.08	3	0.01	0.05	0.03	0.08	3
DMP336	Pure-clinopyroxenite	Bulk rock	0.21	0.05	0.41	0.08	3	-0.05	0.05	-0.06	0.08	3
		Clinopyroxene	0.24	0.05	0.46	0.08	3	-0.05	0.05	-0.08	0.08	3
DMP539	Pure-clinopyroxenite	Bulk rock	0.04	0.05	0.08	0.08	3	-0.27	0.05	-0.42	0.08	3
Replicate		Bulk rock	0.04	0.05	0.09	0.08	3	-0.29	0.05	-0.45	0.08	3
Average		Bulk rock	0.04	0.05	0.08	0.08		-0.28	0.05	-0.44	0.08	
DMP528	“Galssy” xenolith	Bulk rock	0.44	0.05	0.95	0.08	3	0.07	0.05	0.11	0.08	3
Replicate		Bulk rock	0.42	0.05	0.89	0.08	3					
Average		Bulk rock	0.43	0.05	0.92	0.08						
DMP368	Al-websterite	Bulk rock	0.26	0.05	0.53	0.08	3					
DMP382	Al-websterite	Bulk rock	0.30	0.05	0.60	0.08	3					
DMP376	Al-websterite	Bulk rock	0.28	0.05	0.57	0.08	3					
DMP388	Al-websterite	Bulk rock	0.28	0.05	0.55	0.08	3					
DMP369	Al-websterite	Bulk rock	0.25	0.05	0.50	0.08	3					
DMP374	Al-websterite	Bulk rock	0.29	0.05	0.56	0.08	3					
BHVO-2	Basalt	Bulk rock	0.32	0.05	0.62	0.08	3	0.11	0.05	0.15	0.08	3
BCR-2	Basalt	Bulk rock						0.08	0.05	0.13	0.08	3
BIR-1a	Basalt	Bulk rock	0.24	0.05	0.44	0.08	3					
W-2	Diabase	Bulk rock	0.20	0.05	0.43	0.08	3					

Note. *N* represents the times of repeat measurements of the same purified solution by MC-ICP-MS.

#### 4.1.2. Clinopyroxene and Phlogopite

The major and trace element compositions of clinopyroxenes and phlogopites are provided in Table S2 in Supporting Information S1. Clinopyroxenes in the clinopyroxenite xenoliths have the same MgO (13.6–17.5 wt.%), FeO<sub>T</sub> (2.21–5.39 wt.%), Ni (4.49–30.2 ppm), and Cr (4.30–75.5 ppm) contents as whole-rock, and no core-to-rim compositional gradient was observed within individual minerals. Compared to the clinopyroxenes in clinopyroxenites,

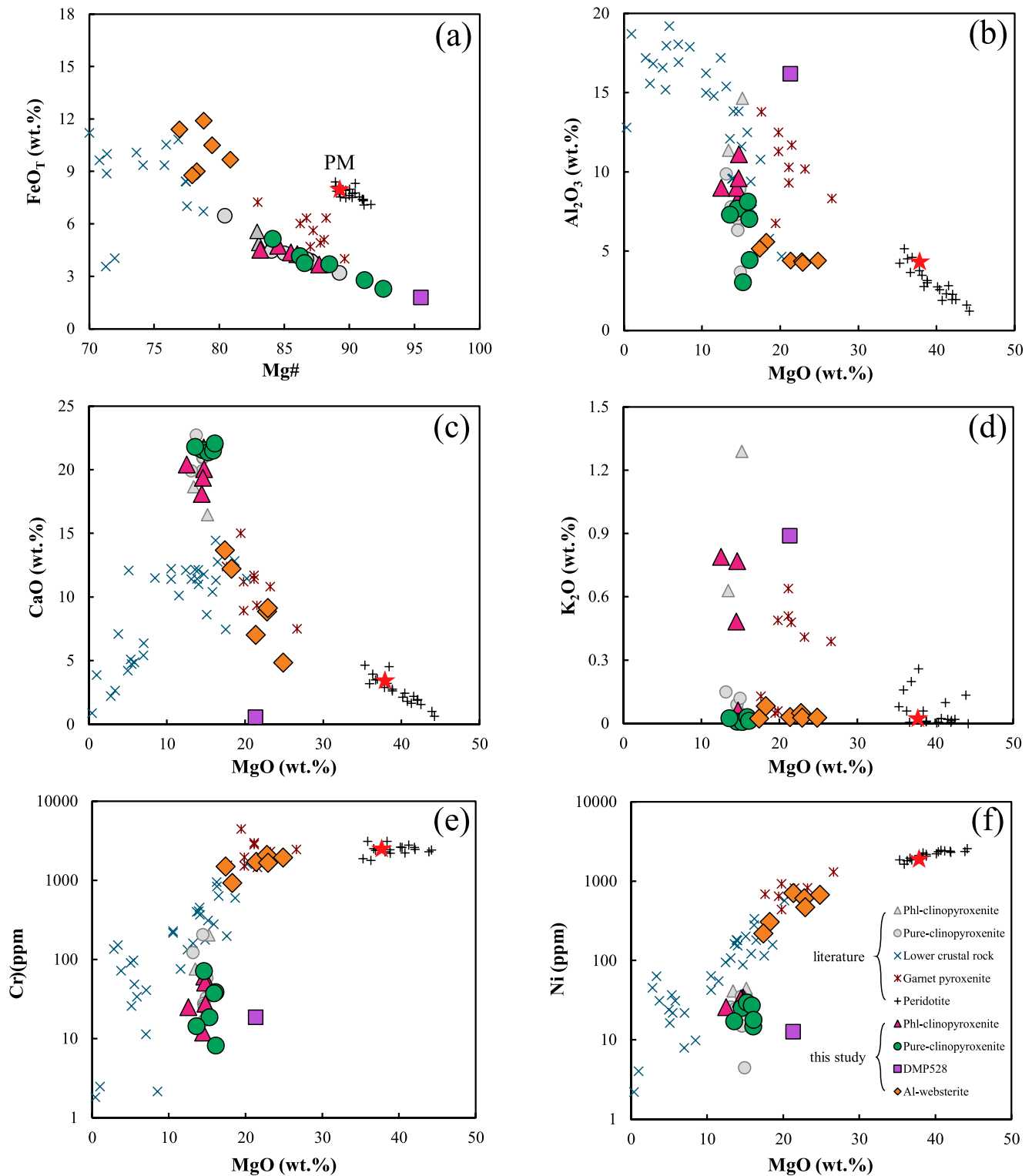


**Figure 2.** Plots of whole-rock Mg# versus  $\text{FeO}_{\text{T}}$  (a); MgO versus  $\text{Al}_2\text{O}_3$  (b), CaO (c),  $\text{K}_2\text{O}$  (d), Cr (e), and Ni (f) for the Hannuoba clinopyroxenites and sample DMP528. Data for Hannuoba garnet pyroxenites (Y. Liu et al., 2005), Al-websterites (this study), peridotites (Y. Liu et al., 2005; Rudnick et al., 2004), and lower crustal xenoliths (Y. Liu et al., 2001; G. Zhang et al., 2020) are plotted for comparison. Literature data of the Hannuoba clinopyroxenites are from Y. Xu (2002), Zheng et al. (2009), Y. Hu et al. (2016), X. Zhao et al. (2017), and J. Hu et al. (2019). The red star represents the composition of the primitive mantle from McDonough and Sun (1995).

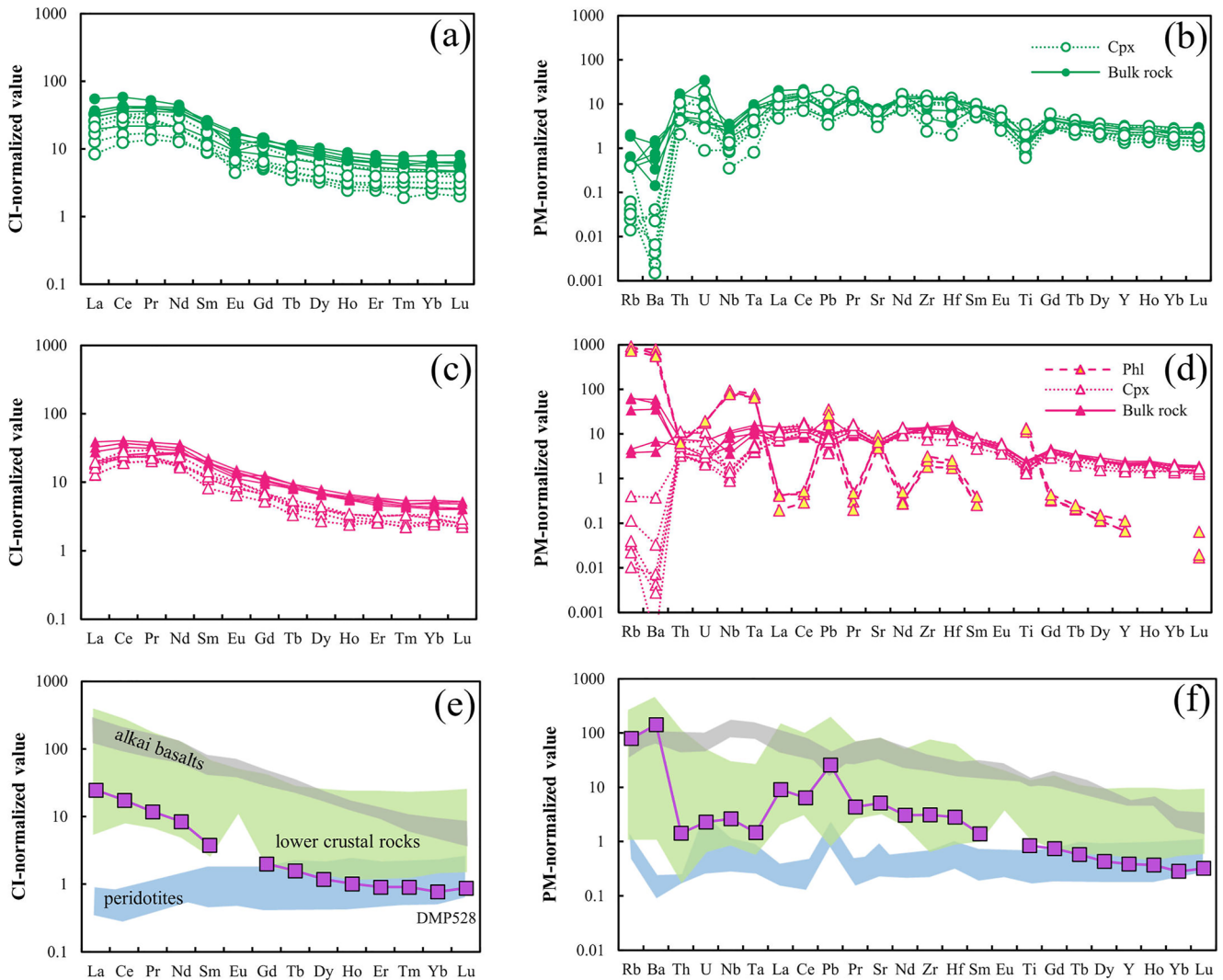


**Figure 3.** Chondrite-normalized rare earth element patterns and PM-normalized trace element patterns for clinopyroxenes and bulk-rock of the clinopyroxenites (a–d) and bulk-rock of sample DMP528 (e, f). The gray, light-green, and light-blue areas represent the compositions of host basalts (Qian et al., 2015), Hannuoba lower crustal xenoliths (Zhang et al., 2020), and peridotite xenoliths (Rudnick et al., 2004), respectively. The normalizing values are from McDonough and Sun (1995). CI, Chondrite. The trace element composition of the clinopyroxene is the average of multiple analysis results.

phlogopites have higher  $\text{Al}_2\text{O}_3$  (16.1–19.0 wt.%) and  $\text{K}_2\text{O}$  (4.47–4.53 wt.%) contents. Also, bulk-rock and clinopyroxenes of the phl-clinopyroxenites show similar distributions in nearly all elements, except for Rb, Ba, Na, and Ta (Figure 3d). Higher concentrations of these elements in bulk-rock are due to the contribution from phlogopite, which is characterized by enrichments in these elements (Figure 3d).

#### 4.2. Zircon U-Pb Ages and Trace Element Compositions

Zircons separated from DMP107 (phl-clinopyroxenites) are prismatic, rounded, or irregular (Figure S1 in Supporting Information S1). The grains are 30–100  $\mu\text{m}$  long with length/width ratios of 1:1 to 2:1 (Figure S1 in Supporting Information S1). Zircon U-Pb ages and trace element compositions are provided in Table S3 in Supporting Information S1. Forty-three zircon grains define a discordia with an upper intercept age of  $1,819 \pm 10$  Ma and a lower intercept age of  $56 \pm 24$  Ma (MSWD = 14; Figure S3 in Supporting Information S1). Analyses with LREE-rich inclusions were eliminated by monitoring the signal variations of trace elements over time. The zircons near the lower intercept age are mostly characterized by enrichments in LREE (Figure S3b in Supporting Information S1). However, other zircons have lower LREE contents and distinctly positive Ce anomalies (Figure S3b in Supporting Information S1).

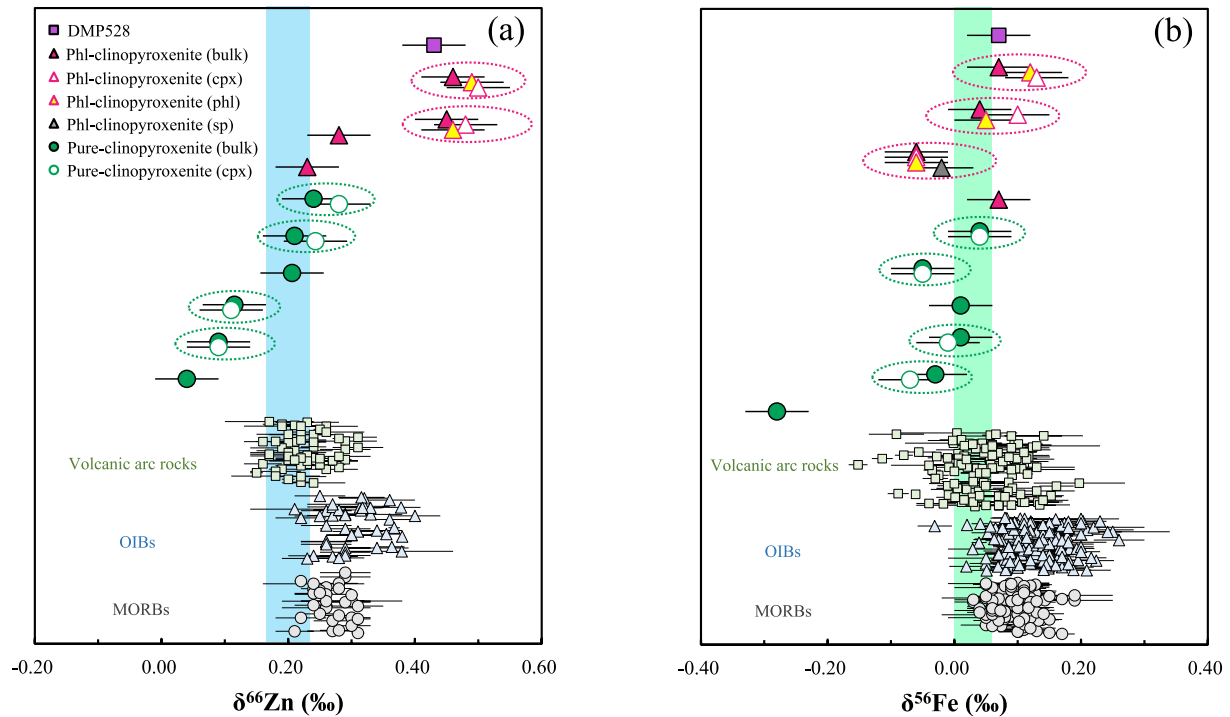


**Figure 4.** Zinc-Fe isotopic compositions of bulk-rock and mineral separates of the clinopyroxenites and sample DMP528. Data for volcanic arc rocks (Z. Chen et al., 2021; Foden et al., 2018; Huang et al., 2018; Nebel et al., 2015), ocean island basalts (Beunon et al., 2020; H. Chen et al., 2013; Konter et al., 2016; Teng et al., 2013; Wang et al., 2017), and mid-ocean ridge basalts (Huang et al., 2018; Teng et al., 2013; Wang et al., 2017) are plotted for comparison. The light blue and light green bars represent the estimated  $\delta^{66}\text{Zn}$  value ( $0.20\text{‰} \pm 0.03\text{‰}$ ) and  $\delta^{56}\text{Fe}$  value ( $0.03\text{‰} \pm 0.03\text{‰}$ ) of Bulk Silicate Earth (Doucet et al., 2020). Error bars represent two standard deviations (2SD).

### 4.3. Strontium-Nd Isotopic Compositions

The  $^{87}\text{Sr}/^{86}\text{Sr}$  ratios of clinopyroxenes in clinopyroxenites show considerable variation between samples from 0.71027 to 0.71566 (except for DMP335). Sample DMP335 has clinopyroxenes with extremely high  $^{87}\text{Sr}/^{86}\text{Sr}$  ratios (0.73080–0.73326). Also, core-rim variations are observed for  $^{87}\text{Sr}/^{86}\text{Sr}$  ratios in some individual minerals (Table S4 in Supporting Information S1).

The clinopyroxenites have low whole-rock  $^{143}\text{Nd}/^{144}\text{Nd}$  ratios from 0.511394 to 0.511688 (Table S5 in Supporting Information S1). Compared to the clinopyroxenites, sample DMP528 has lower  $^{87}\text{Sr}/^{86}\text{Sr}$  and  $^{143}\text{Nd}/^{144}\text{Nd}$  ratios (Table S5 in Supporting Information S1).

### 4.4. Zinc-Fe Isotopic Compositions

Zinc-Fe isotopic ratios of clinopyroxenites, Al-websterites, “glassy” xenolith, and mineral separates from clinopyroxenites are reported in Table 1. The whole-rock  $\delta^{66}\text{Zn}$  values of clinopyroxenite xenoliths range from 0.04‰ to 0.46‰, and their values overlap with the Zn isotopic compositions of mid-ocean ridge basalts (MORBs), ocean island basalts (OIBs) and volcanic arc rocks (Figure 4a). Compared to the Zn isotopic compositions of pure-clinopyroxenites (0.04‰–0.24‰), phl-clinopyroxenites show higher  $\delta^{66}\text{Zn}$  values (0.23‰–0.46‰) (Figure 4a). Mineral separates (clinopyroxene and phlogopite) from clinopyroxenites have similar  $\delta^{66}\text{Zn}$  values to the corresponding whole-rock (Figure 4a). Two clinopyroxene-phlogopite pairs yield  $\Delta^{66}\text{Zn}_{\text{Cpx-Phl}}$  ( $\delta^{66}\text{Zn}_{\text{Cpx}} - \delta^{66}\text{Zn}_{\text{Phl}}$ ) from 0.01‰ to 0.02‰. The Al-websterite xenoliths display a narrow range for  $\delta^{66}\text{Zn}$  values (0.25‰–0.30‰). The “glassy” xenolith has a relatively heavy Zn isotopic composition (0.43‰).

All but one of the clinopyroxenites (DMP539,  $-0.28\text{‰}$ ) have uniform  $\delta^{56}\text{Fe}$  values ranging from  $-0.05\text{‰}$  to 0.07‰ and there is no systematic difference in Fe isotopic composition between pure-clinopyroxenite and phl-clinopyroxenite (Figure 4b). Mineral separates (clinopyroxene, phlogopite, and spinel) from clinopyroxenites have similar  $\delta^{56}\text{Fe}$  values with the corresponding whole-rock (Figure 4b). The inter-mineral Fe isotopic



fractionation ( $\Delta^{56}\text{Fe}_{X-Y} = \delta^{56}\text{Fe}_X - \delta^{56}\text{Fe}_Y$ , where  $X$  and  $Y$  refer to two different mineral phases) varies from 0.00‰ to 0.05‰ between clinopyroxene and phlogopite, 0.04‰ between spinel and clinopyroxene, and 0.04‰ between spinel and phlogopite. Lastly, the “glassy” xenolith has a  $\delta^{56}\text{Fe}$  value of 0.07‰.

## 5. Discussion

### 5.1. Origin of the Hannuoba Clinopyroxenite Xenoliths

Different models have been proposed to account for the chemical and isotopic characteristics of the Hannuoba clinopyroxenites, including basaltic melts accumulation (Y. Xu, 2002; Zheng et al., 2009), melt metasomatism (J. Hu et al., 2019; Y. Hu et al., 2016), and cumulates modified by subsequent metasomatism (X. Zhao et al., 2017; Zong et al., 2005). However, these studies typically focused on specific geochemical characteristics to explain the origin of clinopyroxenites without further explaining the highly variable Ba/Th (0.81–103), Rb/La (0.02–8.12), Li/Y (0.25–1.28), Nb/Ta (5.50–14.4), and Th/Nb (1.05–0.04) ratios (Figure 5). These ratioed elements have nearly identical solid/melt bulk partition coefficients in normal basaltic systems (e.g., Elliott et al., 1997; Kogiso et al., 1997). The bulk-rock Ba/Th and Rb/La ratios of clinopyroxenites show excellent correlations with  $\text{Al}_2\text{O}_3$  and  $\text{K}_2\text{O}$  contents as well as Li/Y, Nb/Ta and Th/Nb ratios (Figure 5). Three possible scenarios could explain the variable chemical compositions of clinopyroxenites: (a) variable degrees of alkaline melt/fluid metasomatism (Fitzpayne et al., 2018; O’Reilly & Griffin, 2013), (b) magmatic cumulates with different modal Phl abundances (Fitzpayne et al., 2018), or (c) different degrees of Phl decomposition of phl-clinopyroxenites with initially same modal Phl contents in an open-system (J. Hu et al., 2019).

Fluid/melt metasomatism can change the chemical and isotopic compositions of mantle minerals (O’Reilly & Griffin, 2013). Lithium and Y contents in Cpx and Phl (Table S2 in Supporting Information S1) and the modal mineral abundances indicate that Li and Y are mainly hosted in Cpx (>95% Li and >99% Y) in these clinopyroxenite xenoliths. Therefore, melts/fluids metasomatism may cause changes in the Li/Y ratio of Cpx, but Phl accumulation and breakdown would not modify the Li/Y ratio of Cpx. Notably, the Li/Y ratios of Cpx show roughly positive correlations with bulk-rock Ba/Th and K/U ratios of the clinopyroxenites (Figure 6). Furthermore, the highly variable  $\delta^{66}\text{Zn}$  values of Cpx from clinopyroxenites and similar Zn isotopic characteristics of Cpx-Phl pairs from phl-clinopyroxenites is not consistent with Phl accumulation and decomposition, because the different modal Phl abundances would not modify the Zn isotopic compositions of Cpx. Moreover, since Th and Nb have low solubility in slab-derived fluids (Kessel et al., 2005), the negative correlation between Th/Nb and Ba/La ratios (Figure 5f) cannot be produced simply by the metasomatic modification of aqueous fluids. Collectively, the variable modal Phl abundances and element ratios (e.g., Ba/Th, Rb/La and Th/Nb) of Hannuoba clinopyroxenites are produced by variable degrees of hydrous melt metasomatism.

Hannuoba clinopyroxenite xenoliths have extremely low Cr and Ni contents compared to other magmatic Al-websterites and metasomatic garnet pyroxenites from the same host basalts (Figures 3e–3f). The nearly constantly low Cr and Ni contents from pure-to phl-clinopyroxenite and the absence of correlation with Ba/Th ratios (Figures S4a and S4b in Supporting Information S1) indicate the low Cr and Ni contents reflect the original composition of the primitive (pre-metasomatized) clinopyroxenite. Chromium and Ni are mainly partitioned into residual mineral phases during low-degree partial melting of mantle peridotites (e.g., Hauri et al., 1994; Mysen, 1978). For example, a mantle xenolith (phlogopite + clinopyroxene + amphibole) crystallized from low-degree mantle-derived ultramafic alkaline melt has low Cr (12–28 ppm) and Ni (26.3–106 ppm) contents of bulk-rock and minerals similar to Hannuoba clinopyroxenites (Smart et al., 2019). Furthermore, convex-upward REE patterns of Hannuoba clinopyroxenites are typical features of cumulate pyroxenites (Figures 3a and 3c) (Zou et al., 2014). And the diverse LREE patterns of the equilibrium melt suggest that clinopyroxenites and Al-websterites were derived from different mantle sources (Figure S5 in Supporting Information S1). Therefore, the clinopyroxenites likely represent accumulated mineral assemblages from low-degree mantle-derived basaltic melts, and then undergo variable degrees of hydrous melt metasomatism (this metasomatic event is referred to as “later-stage metasomatism” in the following).

### 5.2. Timing of Multiple Events Recorded by Clinopyroxenite Xenoliths

Zircon can be used to trace metasomatic events and recycling of crustal materials (J. Hu et al., 2019; Y. Liu et al., 2010). Our zircons from the Hannuoba clinopyroxenites yield an upper intercept age of  $1,819 \pm 10$  Ma

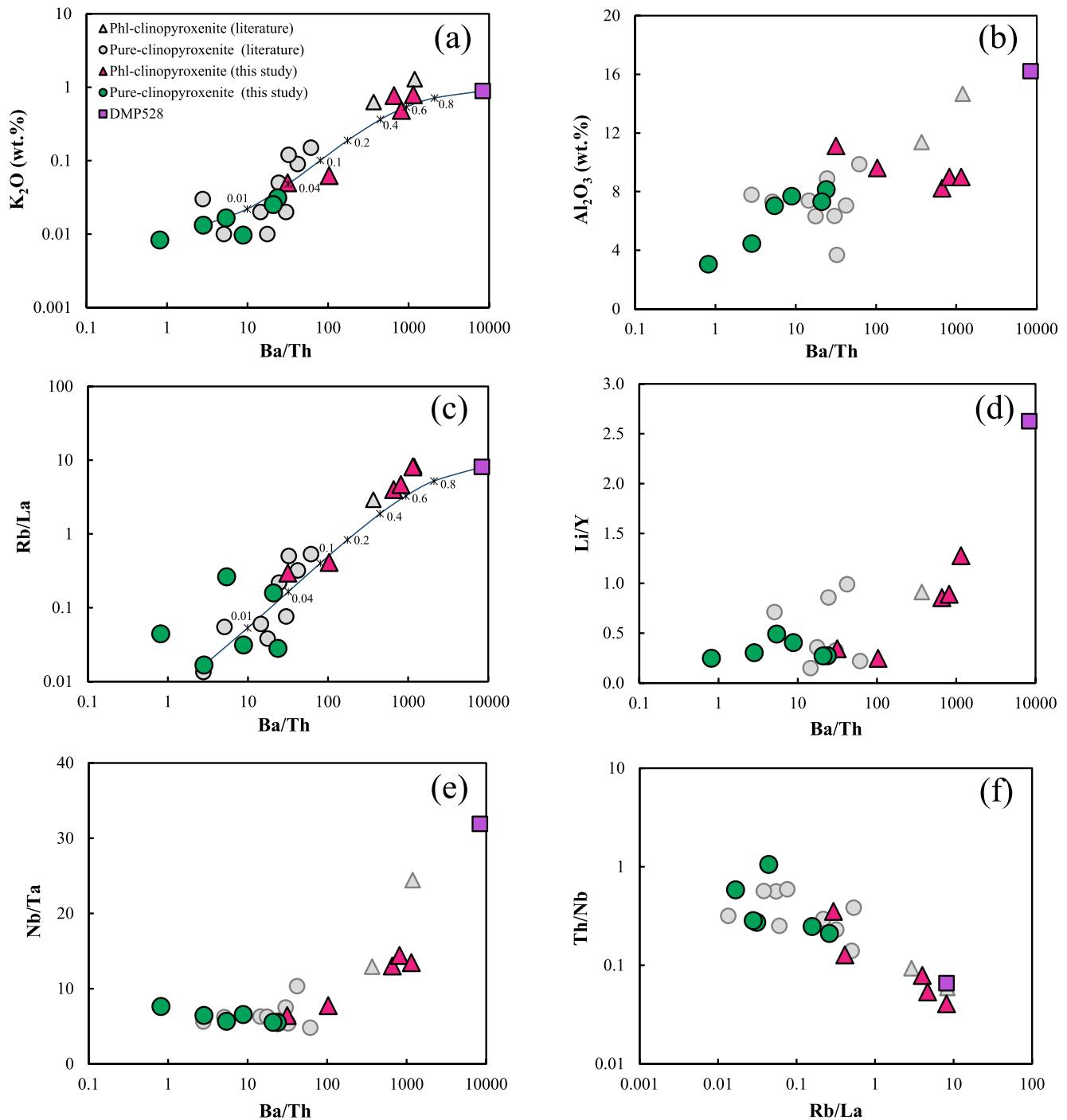


**Figure 5.** Bulk-rock variations of Ba/Th ratios versus  $K_2O$  (a),  $Al_2O_3$  (b), Rb/La (c), Li/Y (d), and Nb/Ta (e) and Rb/La versus Th/Nb ratios (f) for the clinopyroxenites and sample DMP528. The curves in (a) and (c) represent the mixing of sample DMP539 with sample DMP528.

and a lower intercept age of  $56 \pm 24$  Ma (Figure S3 in Supporting Information S1). Zircon from clinopyroxenites could be xenocrysts from the subducted slab or delaminated lower continental crust. J. Hu et al. (2019) also found rare zircons in two Hannuoba clinopyroxenites that yield a wide range of ages (from 92 to 1,911 Ma). Combining their geochronology and O-isotope data, J. Hu et al. (2019) infer that the timing of clinopyroxenite metasomatism was most likely around 320–368 Ma, because only zircons with ages of 320–368 Ma have distinctly high  $\delta^{18}O$  values of 10.20‰–11.34‰ similar to the whole-rock of clinopyroxenites (9.9‰–11.3‰; J. Hu et al., 2019). However, whole-rock of phl- and pure-clinopyroxenites show constantly high  $\delta^{18}O$  values (J. Hu et al., 2019),

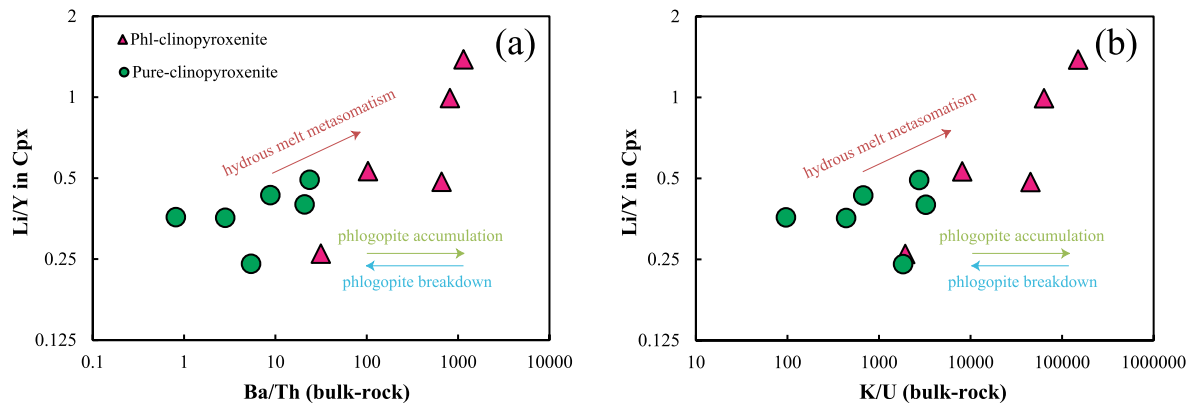


**Figure 6.** Plots of Li/Y ratios of the clinopyroxenes versus Ba/Th (a) and K/U (b) ratios of the bulk-rock for the clinopyroxenites. The Li/Y ratio of each clinopyroxene is the average of multiple analysis results (Table S2 in Supporting Information S1).

indicating that parental melt of clinopyroxenite (i.e., mantle source) contained involved high  $\delta^{18}\text{O}$  crustal materials (see Section 5.3 for a detailed discussion). Therefore, the timing of 320–368 Ma is most likely to represent the time when the mantle source of parental melt for clinopyroxenite interacted with high  $\delta^{18}\text{O}$  crustal materials.

In contrast, zircons with Precambrian ages have  $\delta^{18}\text{O}$  values lower than 7.16‰, which are significantly lower than those of clinopyroxenite whole rocks (J. Hu et al., 2019). Cathodoluminescence images of the Precambrian zircons generally show residual cores with overgrowth rims (Figure S1 in Supporting Information S1). The trace element compositions of the Precambrian zircons are within the range of zircons from continental granitoid rocks (Figures S3c and S3d in Supporting Information S1) (Grimes et al., 2007). These observations indicate that the Precambrian zircons were xenocrysts from the ancient continental crust. The zircons near the lower intercept age generally show well-developed growth zoning and LREE-rich REE patterns (Figure S3 in Supporting Information S1), indicating that they formed by LREE-rich fluid/melt-rock interaction at  $56 \pm 24$  Ma. Additionally, 45–64 Ma zircons were identified in the mafic granulite, websterite and garnet pyroxenite xenoliths from the Hannuoba basalts (Y. Liu et al., 2010; Zheng et al., 2009). The U-Pb isotopic systems of Precambrian zircons in the clinopyroxenites were also reset by the thermal event at  $\sim 56$  Ma (Figure S3 in Supporting Information S1). Therefore, we suggest that the clinopyroxenites have undergone hydrous melt metasomatism at  $\sim 56$  Ma.

### 5.3. Recycled Upper Continental Crust Components in Mantle Source of Clinopyroxenite Xenoliths

Clinopyroxene is a well-suited mineral that provides relevant temporal information (core to rim) about complex geological processes (Schmidberger et al., 2003). The Cpxs from pure- and phl-clinopyroxenite xenoliths display extremely high  $^{87}\text{Sr}/^{86}\text{Sr}$  ratios (0.71027–0.73326). Some individual Cpxs show variable  $^{87}\text{Sr}/^{86}\text{Sr}$  ratios from the core (high) to rim (low) (Figures 7b–7c), excluding the possibility that high  $^{87}\text{Sr}/^{86}\text{Sr}$  ratios in Cpxs are caused by the diffusion of Rb and Sr between Cpx and Phl. These results indicate that the primary Cpxs recorded in the cores have enriched Sr isotopic compositions, and the lower  $^{87}\text{Sr}/^{86}\text{Sr}$  ratios of the rims may be caused by later-stage ( $\sim 56$  Ma) melts/fluids metasomatism.

The clinopyroxenite xenoliths have more radiogenic Sr and less radiogenic Nd isotopic compositions than those of their host basalts and other xenoliths from the same locality, and also MARID (mica-amphibole-rutile-ilmenite-diopside) and PIC (phlogopite-ilmenite-clinopyroxene) xenoliths from South African kimberlites (Figure 7). The Hannuoba pure- and phl-clinopyroxenites also have constantly low  $\delta^{26}\text{Mg}$  ( $-1.04\text{‰}$ – $-1.51\text{‰}$ ) and high  $\delta^{18}\text{O}$  values (9.9‰–11.3‰) (J. Hu et al., 2019; Y. Hu et al., 2016; X. Zhao et al., 2017). Also, continental crust-derived Precambrian zircons have been found in clinopyroxenite xenoliths (J. Hu et al., 2019 and this study). The geochemical evidence of clinopyroxenites indicates the involvement of recycled Mg-rich carbonates (J. Hu et al., 2019; Y. Hu et al., 2016) and ancient continental crust components in their mantle source. Additionally, the enriched Sr-Nd-O isotopic characteristics of clinopyroxenites are inherited from their metasomatized mantle sources.

The geochemical evidence presented above indicates that the Hannuoba clinopyroxenites were formed by the accumulation and crystallization of melts from enriched mantle sources (enriched Sr-Nd-O isotopic compositions).

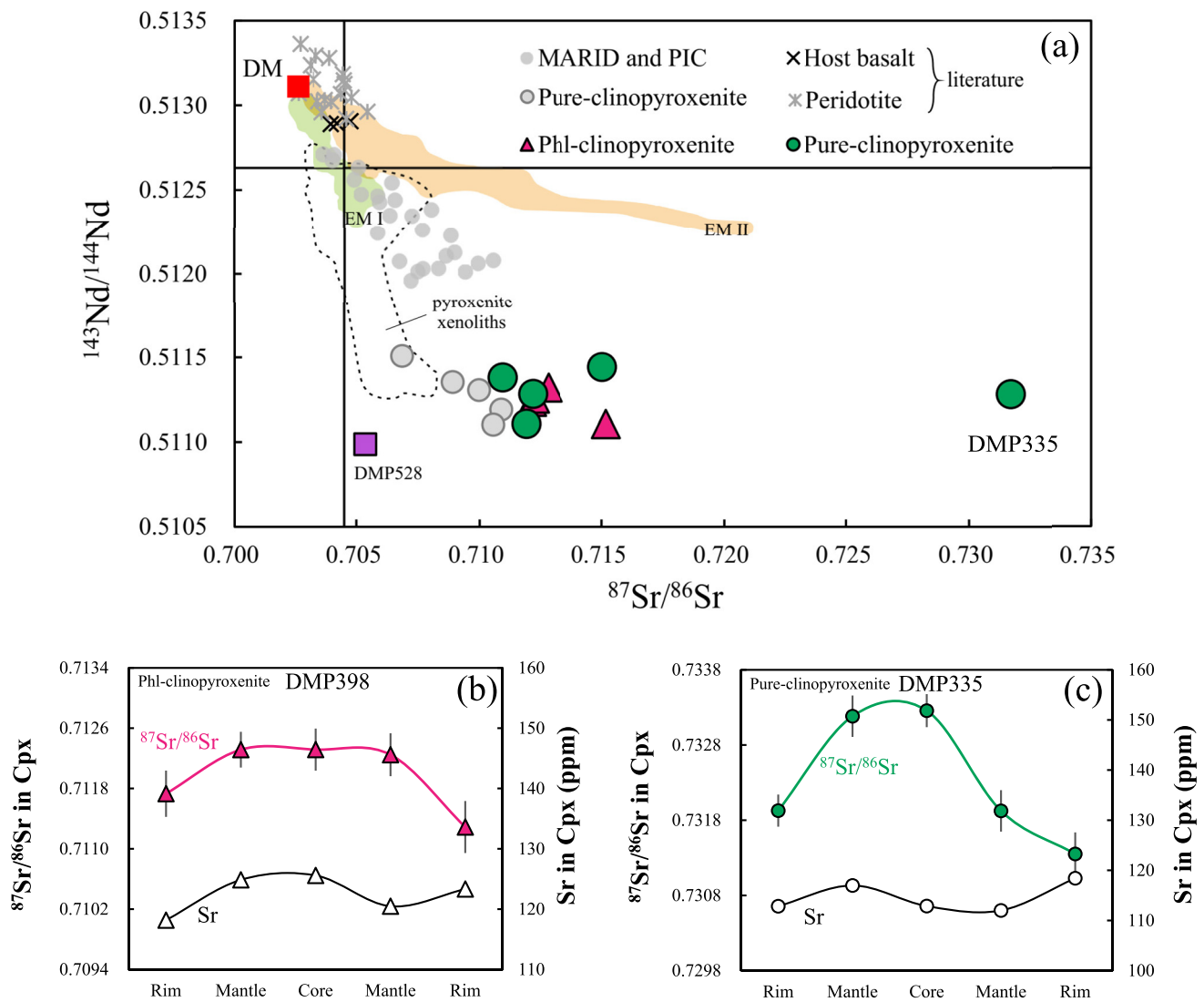


**Figure 7.** (a) A plot of  $^{87}\text{Sr}/^{86}\text{Sr}$  ratios versus  $^{143}\text{Nd}/^{144}\text{Nd}$  ratios of Hannuoba clinopyroxenites and sample DMP528. The  $^{87}\text{Sr}/^{86}\text{Sr}$  ratio of Cpx is used as a proxy for the Sr isotopic composition of the whole-rock of Hannuoba clinopyroxenite (this study). The  $^{87}\text{Sr}/^{86}\text{Sr}$  ratios (whole-rock) of Hannuoba clinopyroxenites from literature and  $^{143}\text{Nd}/^{144}\text{Nd}$  ratios (whole-rock) of all clinopyroxenites were recalculated to 340 Ma (J. Hu et al., 2019). The DM (depleted mantle; Salters & Stracke, 2004), EM I (enriched mantle I; Pitcairn islands; <http://georoc.mpch-mainz.gwdg.de/georoc>), EM II (enriched mantle II; Samoa islands; <http://georoc.mpch-mainz.gwdg.de/georoc>), MARID and PIC xenoliths (Fitzpayne et al., 2019), DMP528 (this study), pure-clinopyroxenite (J. Hu et al., 2019; Y. Xu, 2002), host basalts (Tatsumoto et al., 1992), other Hannuoba pyroxenites (J. Hu et al., 2019; Y. Xu, 2002; X. Zhao et al., 2017) and peridotites (Rudnick et al., 2004) are shown for comparison. The  $^{87}\text{Sr}/^{86}\text{Sr}$  ratios of each clinopyroxenite are the average of multiple analysis results (Table S4 in Supporting Information S1). (b, c) Variations of Sr contents and  $^{87}\text{Sr}/^{86}\text{Sr}$  ratios across clinopyroxene grains from the phl-clinopyroxenite (DMP398) and pure-clinopyroxenites (DMP335). Error bars represent  $2\sigma$ .

Subsequently, these clinopyroxenites underwent varying degrees of later-stage melt/fluid melt metasomatism. The Ba/Th ratio can be used as a geochemical proxy to determine the degree of later-stage metasomatism (Figure 5). Consequently, it is justifiable to constrain the chemical compositions of the parental melt by utilizing the clinopyroxenites with the lowest Ba/Th ratios (DMP539, except for DMP335; Figure 5), which represents the least later-stage metasomatized sample. Since the upper and lower continental crust has negative and slightly positive Eu anomalies (Rudnick & Gao, 2014), respectively, the negative Eu anomalies of sample DMP539 ( $\text{Eu}/\text{Eu}^* = 0.52$ ) indicate that its mantle source may have incorporated subducted upper crustal components. In PM-normalized trace element diagrams, bulk-rock and clinopyroxenes of sample DMP539 are characterized by enriched in Th, U, and LREE but depleted in Rb, Ba, Nb, Ta, Zr, Hf, and Ti (Figure 3b). Furthermore, Rb and Ba are fluid-mobile elements, while Th is mobilized in sediment melts (Elliott et al., 1997; Kessel et al., 2005), indicating that recycled sediment components enter the mantle source of clinopyroxenites as melts rather than

aqueous fluids. Collectively, the geochemical evidence of clinopyroxenites suggests that their mantle source may involve recycled Mg-rich carbonate (J. Hu et al., 2019; Y. Hu et al., 2016) and ancient upper continental crust components.

#### 5.4. Origin of Fe and Zn Isotopic Variations in the Clinopyroxenite Xenoliths

Clinopyroxenite xenoliths show a wide range of  $\delta^{66}\text{Zn}$  values (0.04‰–0.46‰) and relatively constant  $\delta^{56}\text{Fe}$  values ranging from  $-0.05\text{‰}$  to  $0.07\text{‰}$  (except for DMP539,  $-0.28\text{‰}$ ). Several geological processes may account for this, including magmatic processes (mantle partial melting and magmatic differentiation), mantle source heterogeneity, and later-stage melt/fluid metasomatism. To explore the Zn-Fe isotopic characteristics of the clinopyroxenites, we need to evaluate all processes that could have potentially affected the evolution of the Zn-Fe isotopic systematics of the clinopyroxenite xenoliths.

##### 5.4.1. Magmatic Processes

Previous studies of natural samples, experiments, and theoretical models indicate that mantle partial melting can fractionate Zn and Fe isotopes, but the magnitude of Zn and Fe isotopic fractionations are known to be small ( $\Delta^{66}\text{Zn}_{\text{melt-mantle}} < 0.1\text{‰}$  and  $\Delta^{56}\text{Fe}_{\text{melt-mantle}} < 0.1\text{‰}$ ) (Dauphas et al., 2009; Sossi et al., 2016, 2018; Wang et al., 2017; Williams & Bizimis, 2014). Recently, Day et al. (2022) showed that different extents of partial melting of variably fertile and refractory peridotite mantle sources can cause large Zn isotopic variations. However, this process fails to form samples with low (0.04‰) and high (0.46‰)  $\delta^{66}\text{Zn}$  values. Therefore, partial melting of a normal homogeneous peridotitic mantle is insufficient to explain Zn-Fe isotopic characteristics of the clinopyroxenites.

Crystallization of isotopically light olivine and Fe-Ti oxides may shift the differentiated melts and cumulates toward heavier and lighter Zn isotopic compositions relative to the primitive melts, respectively (H. Chen et al., 2013; Yang & Liu, 2019; G. Zhang et al., 2020). However, the lack of resolvable Zn isotopic fractionation in the Kamchatka-Aleutian arc rocks and South China Sea basalts (MgO: 2.2–16.7 wt.%), which are related to the fractionation and accumulation of olivine and pyroxene, indicating that magma differentiation has an insignificant effect on the Zn isotopic compositions of these magmatic rocks (Huang et al., 2018). This is consistent with the constant  $\delta^{66}\text{Zn}$  values of Al-websterite xenoliths (0.25‰–0.30‰), although they have undergone variable degrees of olivine, orthopyroxene, and clinopyroxene accumulation (Figures 8a–8c). For clinopyroxenite xenoliths,  $\delta^{66}\text{Zn}$  values do not show any correlation with magmatic differentiation indexes such as MgO,  $\text{FeO}_{(\text{T})}$ , or Cr contents (Figures 8a–8c). Additionally, the  $\delta^{66}\text{Zn}$  values of sample DMP138 with spinel are indistinguishable from that of sample DMP340, although both have experienced the same degree of melt metasomatism. The above evidence suggests that mineral fractionation and accumulation have a limited influence on Zn isotopic fractionation of the clinopyroxenites. Furthermore, the absence of any correlation between  $\delta^{56}\text{Fe}$  and MgO,  $\text{FeO}_{(\text{T})}$ , and Cr contents (Figures 8d–8f) suggests the Fe isotopic variation within the Hannuoba clinopyroxenites is not controlled by mineral accumulation but could be attributed to other geological processes.

##### 5.4.2. Mantle Source Heterogeneity and Later-Stage Melt/Fluid Metasomatism

The addition of sediments in mantle source and melt/fluid metasomatism could modify the Zn-Fe isotopic compositions of the mantle-derived rocks (e.g., Huang et al., 2019; Konter et al., 2016; S.-A. Liu et al., 2016; R. Xu et al., 2022; X. Zhao et al., 2017). The clinopyroxenites show a narrow range of  $\delta^{56}\text{Fe}$  values ( $-0.05\text{‰}$ – $0.07\text{‰}$ ) around the estimated value of Bulk Silicate Earth (Figures 8d–8f), except for two outliers: a pure-clinopyroxenite ( $-0.28\text{‰}$ ; this study) and a phl-clinopyroxenite (0.66‰; X. Zhao et al., 2017). There is no correlation between the  $\delta^{56}\text{Fe}$  values and Rb/La, K/U, Ba/Th, and Th/Nb ratios of clinopyroxenites (Figure S6 in Supporting Information S1), indicating that later-stage melt metasomatism did not affect the Fe isotopic compositions of clinopyroxenites. Additionally, clinopyroxenites with  $\text{FeO}_{(\text{T})}$  contents similar to the two outliers have normal  $\delta^{56}\text{Fe}$  values (Figure 8e), suggesting that kinetic fractionation caused by later-stage melt metasomatism cannot explain the observed abnormal  $\delta^{56}\text{Fe}$  values. Therefore, the distinct Fe isotopic compositions of these two clinopyroxenites are most likely inherited from their heterogeneous mantle sources, such as addition of recycled crustal sediments or mantle metasomatism, but more research is needed to confirm this viewpoint.

As the degree of melt/fluid metasomatism increases from pure-clinopyroxenite to phl-clinopyroxenite, their Rb/La, K/U and Ba/Th ratios gradually increase, and Th/Nb ratios gradually decrease (Figure 9). Compared to the Zn

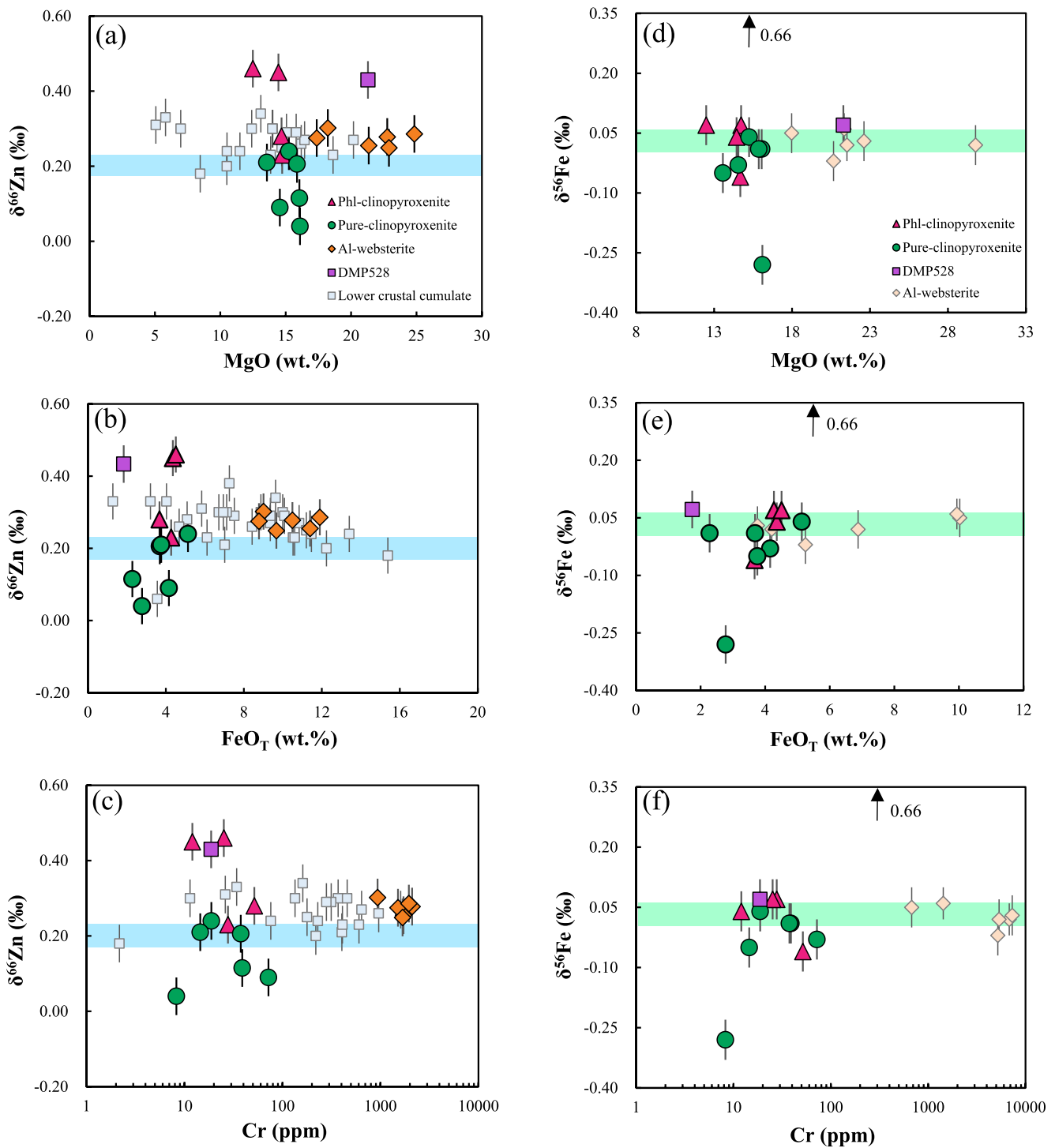


**Figure 8.** Bulk-rock variations of  $\delta^{66}\text{Zn}$  and  $\delta^{56}\text{Fe}$  versus  $\text{MgO}$  (a, d),  $\text{FeO}_T$  (b, e), and  $\text{Cr}$  (c, f) ratios for the clinopyroxenites and sample DMP528. Data for Al-websterites (X. Zhao et al., 2017); this study) and lower crustal cumulates (G. Zhang et al., 2020) are plotted for comparison. The light blue and light green bars represent the estimated  $\delta^{66}\text{Zn}$  value ( $0.20\text{‰} \pm 0.03\text{‰}$ ) and  $\delta^{56}\text{Fe}$  value ( $0.03\text{‰} \pm 0.03\text{‰}$ ) of Bulk Silicate Earth (Doucet et al., 2020). Error bars represent two standard deviations (2SD).

isotopic compositions of pure-clinopyroxenites ( $0.04\text{‰}$ – $0.24\text{‰}$ ), phl-clinopyroxenites show higher  $\delta^{66}\text{Zn}$  values ( $0.23\text{‰}$ – $0.46\text{‰}$ ) (Figure 9). Furthermore, the whole-rock  $\delta^{66}\text{Zn}$  values of clinopyroxenites show excellent correlations with Rb/La, K/U, Ba/Th, and Th/Nb ratios (Figure 9). Mineral separates (clinopyroxene and phlogopite)

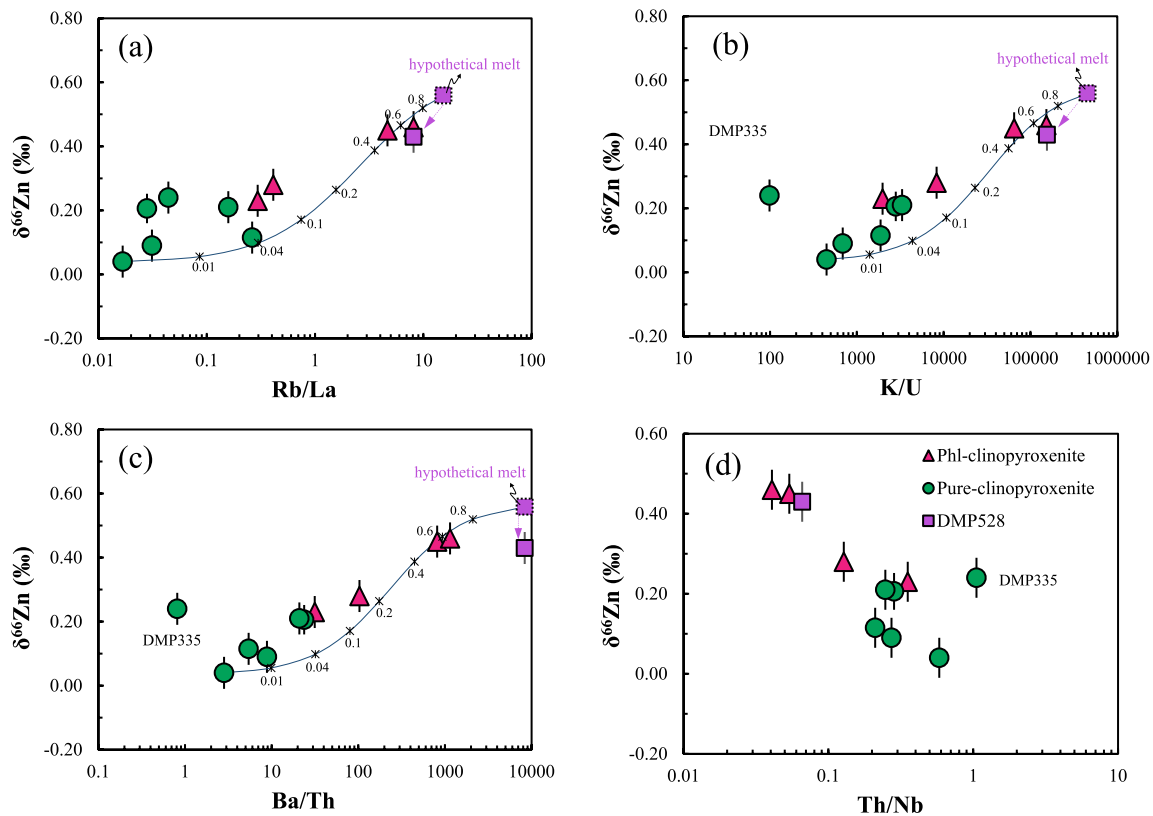


**Figure 9.** Bulk-rock variations of  $\delta^{66}\text{Zn}$  versus Ba/Th (a), K/U (b), Rb/La (c), and Th/Nb (d) ratios for the clinopyroxenites and sample DMP528. The curves represent the mixing of sample DMP539 with a hypothetical metasedimentary melt. The hypothetical metasedimentary melt as an end-member with higher  $\text{K}_2\text{O}$  (2.8 wt.%), Rb (90 ppm), Zn (240 ppm) contents and  $\delta^{66}\text{Zn}$  value (0.56‰) compared to DMP528.

from clinopyroxenites have the same  $\delta^{66}\text{Zn}$  values with their corresponding whole-rock (Figure 4a). Additionally, the difference in Zn isotopic composition ( $\Delta^{66}\text{Zn}_{\text{Cpx-Phl}}$ ) between clinopyroxene and phlogopite from the same phl-clinopyroxenite is 0.01‰–0.02‰, consistent with theoretical calculations ( $\sim 0\%$ ; Fang et al., 2022). This indicates that equilibrium inter-mineral fractionation in clinopyroxenites has been achieved, which is ruling out the possibility of kinetic isotope fractionation during melt-rock interaction as the cause of the clinopyroxenitic isotopic compositions. Consequently, the later-stage melt metasomatism could account for the Zn isotopic variations of clinopyroxenites.

The clinopyroxenites with the lowest degree of melt metasomatism can better reflect the geochemical characteristics of their mantle source. The clinopyroxenite (DMP539) with the lowest Ba/Th ratios has the lightest Zn isotopic compositions (excluding DMP335 with anomaly high  $^{87}\text{Sr}/^{86}\text{Sr}$  ratio), which is significantly lower than the estimated value ( $0.20\text{‰} \pm 0.03\text{‰}$ ; Doucet et al., 2020) of Bulk Silicate Earth (Figure 4a). Furthermore, considering that mantle partial melting would slightly enrich the melt with heavy Zn isotopic compositions (e.g., Sossi et al., 2018; Wang et al., 2017), the mantle source of parental melts for clinopyroxenites should have a lighter Zn isotopic composition ( $< 0.04\text{‰}$ ). Recently, Shu et al. (2023) revealed that recycled carbonate-bearing silicate sediments could induce Mg-Zn isotopic decoupling in mantle-derived magmas, especially in the case of low carbonate fractions in the sediments. Continental margin sediments ( $0.07\text{‰} \pm 0.11\text{‰}$ ; Little et al., 2016) have a significantly lighter Zn isotopic signature than normal mantle, and these sediments can be incorporated into the continental mantle through subduction erosion (Straub et al., 2020). Therefore, the light Zn isotopic compositions of continental margin sediments can potentially overprint the heavy isotopic compositions of carbonates, which is a possible mechanism for the Mg-Zn isotopic decoupling in the mantle sources of clinopyroxenites ( $\delta^{26}\text{Mg}$ :  $-1.53\text{‰}$ – $-1.04\text{‰}$ ; J. Hu et al., 2019; Y. Hu et al., 2016;  $\delta^{66}\text{Zn}$ :  $< 0.04\text{‰}$  in this study).

Previous studies have shown that melts/fluids released from subducted slabs show fractionated Zn and Fe isotopic characteristics (Debret et al., 2016, 2018, 2021; Pons et al., 2016). The heavy Zn isotopic compositions

of chlorite-bearing harzburgite from the Cerro del Almiraz massif were interpreted as external carbonate-bearing fluid percolation, but these samples lack Fe isotope variation (Debret et al., 2021). The decoupled nature of the Zn-Fe isotope variations in Cerro del Almiraz samples was explained by the dissolution and mobility of Zn-rich and Fe-poor carbonates in high-pressure fluids during subduction (Debret et al., 2021). The Rb/La, K/U, Ba/Th, and Th/Nb ratios of Hannuoba clinopyroxenites are correlated with their  $\delta^{66}\text{Zn}$  values but do not correlate with  $\delta^{56}\text{Fe}$  values (Figure 9; Figure S6 in Supporting Information S1), indicating that melt/fluid metasomatism causes the fractionation of Zn isotopes while Fe isotopes remain unchanged. The most likely reason is the similar Fe isotopic compositions between metasomatic agents and clinopyroxenites (Figure S6 in Supporting Information S1). Therefore, from the Zn-Fe isotopic perspective of clinopyroxenites, Zn isotopes have a better potential for tracing later-stage melt/fluid metasomatism of clinopyroxenites.

### 5.5. Slab-Derived Sediment Melt Activity in the Sub-Continental Lithosphere

Decoding the interaction between subduction-related fluids/melts with rocks from the crust-mantle boundary and upper mantle is key to reconstructing lithospheric evolution (O'Reilly & Griffin, 2013). In most studies, the nature of metasomatic fluids/melts was inferred from the chemical compositions (especially trace-element) of minerals and bulk-rock (e.g., Y. Liu et al., 2005; R. Xu et al., 2013; Zou et al., 2014), and only a few cases allow us to directly study the metasomatic agents (Borghini et al., 2018; Schiano et al., 1995). Some glass in lower crustal and mantle rocks can provide direct evidence for the recycling of crustal materials and fluid/melt metasomatism (Borghini et al., 2018; Schiano et al., 1995). A peculiar “glassy” xenolith (fossilized melt; DMP528) was found in Hannuoba basalts. It has major and trace element compositions completely different from the host basalts (Figure 2). More notably,  $\text{Al}_2\text{O}_3$  and  $\text{K}_2\text{O}$  contents, Ba/Th, Rb/La, Li/Y and Nb/Ta ratios and  $\delta^{66}\text{Zn}$  values in clinopyroxenites generate arrays that trend toward a composition similar to sample DMP528 (Figures 5 and 9). Furthermore, core-rim variation of  $^{87}\text{Sr}/^{86}\text{Sr}$  ratio is observed in clinopyroxene crystals, indicating that the  $^{87}\text{Sr}/^{86}\text{Sr}$  ratio of the later-stage metasomatic agent is lower than that of clinopyroxenites (Figures 7b and 7c). These geochemical characteristics of “glassy” xenolith indicate that it may represent a preserved metasomatic melt responsible for the metasomatism of clinopyroxenite xenoliths. Two end-member mixing calculations were used to evaluate the degrees of clinopyroxenites metasomatized by later-stage melt. For this calculation, we use the composition of the sample DMP539 to represent the pre-metasomatized end-member and sample DMP528 as the other end-member (metasomatic melt). Based on simulation results, the later-stage melt metasomatism of clinopyroxenites ranges from 0% to 70% (Figures 5a and 5c). However, an end-member melt with higher  $\text{K}_2\text{O}$ , Rb and Zn contents and  $\delta^{66}\text{Zn}$  value is required to reproduce the  $\delta^{66}\text{Zn}$  trends of clinopyroxenites (Figures 9a–9c). The chemical compositions of “glassy” xenolith may have been slightly modified by mantle rocks. Collectively, these geochemical characteristics of “glassy” xenolith indicate that it may represent a slightly modified metasomatic agent responsible for the metasomatism of clinopyroxenite xenoliths.

Compared with the lower crust xenoliths (chemical compositions from mafic to felsic) carried by the host basalts at the same locality (Y. Liu et al., 2001; G. Zhang et al., 2020), sample DMP528 has significantly higher MgO and lower CaO contents and higher  $\delta^{66}\text{Zn}$  value (Figures 2 and 8a–8c). Therefore, the possibility that it is merely formed by melting of delaminated lower continental crust can be ruled out. Phengite is the main host for the large ion lithophile elements (LILE) in subducted sediments (Hermann & Rubatto, 2009). Based on high-pressure experimental data by Stepanov and Hermann (2013), phengite can also be a significant host for Nb in metamorphic rocks and can fractionate Nb from Ta. The progressive melting of phengite-bearing restites may lead to the enrichment of K, Rb, Ba, and Nb contents and a high Nb/Ta ratio in the sample DMP528 (Stepanov & Hermann, 2013). Furthermore, the high MgO content (21.29 wt.%) and presence of large orthopyroxenes in sample DMP528 indicate that it may be the product of a metasomatic reaction between siliceous melt/fluid and Mg-rich mantle rock. However, the Cr and Ni contents of sample DMP528 are much lower than that of garnet pyroxenites produced by melt-peridotite reactions (Figures 2e and 2f) (Y. Liu et al., 2005), which excludes the possibility that its high MgO content is inherited from the Mg-rich mantle rock. Considering that sedimentary carbonates have heavy Zn isotopic compositions (S.-A. Liu & Li, 2019; S.-A. Liu et al., 2022), the high  $\delta^{66}\text{Zn}$  value (0.43‰) and MgO content of sample DMP528 are more likely to be caused by the involvement of high-Mg carbonates (e.g., magnesite). Combined with a lower  $^{143}\text{Nd}/^{144}\text{Nd}$  ratio (0.510991) of sample DMP528 compared to alter oceanic crust and seawater (Hauff et al., 2003), this evidence mentioned above indicates that it may represent a fossilized sediment melt formed by the melting of metasediments (containing high-Mg carbonates and phengite) with upper continental crust components (radiogenic Nd isotopic composition). To model the



composition of sample DMP528, a simple assumption was made that the MgO in the sample was completely inherited from magnesite, the obtained carbonate and silicate proportions in DMP528 are 45% and 55%, respectively. Magnesite (Zn: 449 ppm,  $\delta^{66}\text{Zn}$ : 0.9‰; S.-A. Liu et al., 2020) and continental upper crust (Zn: 67 ppm,  $\delta^{66}\text{Zn}$ : 0.28‰; Moynier et al., 2017; Rudnick & Gao, 2014) were used to represent carbonate and silicate components, respectively. By mixing these components in the aforementioned ratios, the resulting Zn content (239 ppm) and  $\delta^{66}\text{Zn}$  value (0.559‰) were found to be similar to the hypothetical metasomatic melts mentioned earlier (see Figures 9a–9c).

Subduction of terrigenous clastic sediments and carbonates provides a mechanism by which crustal materials are incorporated into the overlying lithosphere and/or a more in-depth section of the mantle. Growing evidence suggests that chemical and isotopic compositions of oceanic basalts, intraplate basalts, and mantle-derived xenoliths record signatures from a sediment-influenced mantle source (Conticelli et al., 2015; Fitzpayne et al., 2019; Jackson et al., 2007). Notably, an estimated 76 wt.% of subducted sediment has a terrigenous origin (Plank & Langmuir, 1998), and thus subducted sediment contributes a signature of upper continental crust to the mantle. However, mantle-derived rocks with geochemical signatures of recycled upper continental crust are rarely found. A prominent example is the Samoan lavas: the elevated  $^{87}\text{Sr}/^{86}\text{Sr}$  ratios recorded in whole-rock (0.720469), clinopyroxene (0.723888), and plagioclase (0.7224) point to the presence of a high fraction (5%–7%) of recycled upper continental crust component in the Samoan mantle plume (Adams et al., 2021; Edwards et al., 2019; Jackson et al., 2007). The enriched Sr isotopic compositions (up to 0.73326) and upper continental crust (UCC)-like trace-element characteristics of Hannuoba clinopyroxenites in this study suggest the involvement of ancient upper continental crust components in their mantle source. Furthermore, the later-stage metasomatic agent of clinopyroxenites – sample DMP528, represents a fossilized melt formed by the melting of sediments (containing high-Mg carbonates and upper continental crust in the form of silicic components). These studies prove that recycled upper continental crust components may have been incorporated into the lithospheric or asthenospheric mantle through slab subduction. It is also demonstrated that although the contribution of the ambient mantle may significantly dilute the geochemical signatures of recycled crust, upper continental crust components may still be preserved in low abundance in the crust–mantle boundary and the mantle (Adams et al., 2021; Jackson et al., 2007; this study). The identification of “sediment melt” xenolith provides direct insights into the activity of slab-derived sediment melt in the sub-continental lithosphere.

## 6. Conclusions

The main conclusions of this study on the Hannuoba clinopyroxenites and a “glassy” xenolith are:

1. The Hannuoba clinopyroxenite xenoliths are cumulates crystallized from basaltic melts produced by an enriched mantle source with recycled upper continental crust components, and then undergo variable degrees of hydrous melt metasomatism at ~56 Ma.
2. The Zn isotopic variations of the clinopyroxenites are produced by later-stage hydrous melt metasomatism. Moreover, the Fe isotopic variations of clinopyroxenites are most likely caused by mantle source heterogeneity.
3. The covariation of  $\delta^{66}\text{Zn}$  values and Rb/La, K/U, Ba/Th, and Th/Nb ratios of clinopyroxenites indicate that “glassy” xenolith may represent the metasomatic agent responsible for the later-stage hydrous melt metasomatism of clinopyroxenites. It may represent a solidified sediment melt formed by melting of carbonate-bearing terrigenous sediments. This study suggests that Zn isotopes can be used to trace the activity of slab-derived sediment melts in the sub-continental lithosphere.

### Acknowledgments

We gratefully acknowledge Editor Mark Dekkers and Associate Editor Fang-Zhen Teng for their efficient handling and insightful comments. We also thank Jian Huang and two anonymous reviewers for their thorough and constructive reviews. This research is co-supported by the Key R&D Program of China (2019YFA0708400), the National Natural Science Foundation of China (41530211), the MOST Special Funds of the State Key Laboratory of Geological Processes and Mineral Resources (MSFGPMR01).

### Data Availability Statement

Supplementary data are provided in supporting information and are available at zenodo (<https://doi.org/10.5281/zenodo.7340339>).

### References

- Adams, J. V., Jackson, M. G., Spera, F. J., Price, A. A., Byerly, B. L., Seward, G., & Cottle, J. M. (2021). Extreme isotopic heterogeneity in Samoan clinopyroxenes constrains sediment recycling. *Nature Communications*, 12(1), 1234. <https://doi.org/10.1038/s41467-021-21416-9>
- Beunon, H., Mattielli, N., Doucet, L. S., Moine, B., & Debret, B. (2020). Mantle heterogeneity through Zn systematics in oceanic basalts: Evidence for a deep carbon cycling. *Earth-Science Reviews*, 205, 103174. <https://doi.org/10.1016/j.earscirev.2020.103174>

- Borghini, A., Ferrero, S., Wunder, B., Laurent, O., O'Brien, P. J., & Ziemann, M. A. (2018). Granitoid melt inclusions in orogenic peridotite and the origin of garnet clinopyroxenite. *Geology*, *46*(11), 1007–1010. <https://doi.org/10.1130/G45316.1>
- Chen, H., Savage, P. S., Teng, F.-Z., Helz, R. T., & Moynier, F. (2013). Zinc isotope fractionation during magmatic differentiation and the isotopic composition of the bulk Earth. *Earth and Planetary Science Letters*, *369*–370, 34–42. <https://doi.org/10.1016/j.epsl.2013.02.037>
- Chen, Z., Chen, J., Zeng, Z., Soh Tamehe, L., Zhang, T., Zhang, Y., et al. (2021). Zinc isotopes of the Mariana and Ryukyu arc-related lavas reveal recycling of forearc serpentinites into the subarc mantle. *Journal of Geophysical Research: Solid Earth*, *126*(11), e2021JB022261. <https://doi.org/10.1029/2021jb022261>
- Coticelli, S., Avanzinelli, R., Ammannati, E., & Casalini, M. (2015). The role of carbon from recycled sediments in the origin of ultrapotassic igneous rocks in the Central Mediterranean. *Lithos*, *232*, 174–196. <https://doi.org/10.1016/j.lithos.2015.07.002>
- Dauphas, N., Craddock, P. R., Asimow, P. D., Bennett, V. C., Nutman, A. P., & Ohnenstetter, D. (2009). Iron isotopes may reveal the redox conditions of mantle melting from Archean to Present. *Earth and Planetary Science Letters*, *288*(1–2), 255–267. <https://doi.org/10.1016/j.epsl.2009.09.029>
- Day, J. M. D., Moynier, F., & Ishizuka, O. (2022). A partial melting control on the Zn isotope composition of basalts. *Geochemical Perspectives Letters*, *23*, 11–16. <https://doi.org/10.7185/geochemlet.2230>
- Debre, B., Bouilhol, P., Pons, M. L., & Williams, H. (2018). Carbonate transfer during the onset of slab devolatilization: New insights from Fe and Zn stable isotopes. *Journal of Petrology*, *59*(6), 1145–1166. <https://doi.org/10.1093/petrology/egy057>
- Debre, B., Garrido, C. J., Pons, M. L., Bouilhol, P., Inglis, E., López Sánchez-Vizcaíno, V., & Williams, H. (2021). Iron and zinc stable isotope evidence for open-system high-pressure dehydration of antigorite serpentinite in subduction zones. *Geochimica et Cosmochimica Acta*, *296*, 210–225. <https://doi.org/10.1016/j.gca.2020.12.001>
- Debre, B., Millet, M. A., Pons, M. L., Bouilhol, P., Inglis, E., & Williams, H. (2016). Isotopic evidence for iron mobility during subduction. *Geology*, *44*(3), 215–218. <https://doi.org/10.1130/g37565.1>
- Deng, J., He, Y., Zartman, R. E., Yang, X., & Sun, W. (2022). Large iron isotope fractionation during mantle wedge serpentinization: Implications for iron isotopes of arc magmas. *Earth and Planetary Science Letters*, *583*, 117423. <https://doi.org/10.1016/j.epsl.2022.117423>
- Doucet, L. S., Laurent, O., Ionov, D. A., Mattielli, N., Debaille, V., & Debouge, W. (2020). Archean lithospheric differentiation: Insights from Fe and Zn isotopes. *Geology*, *48*(10), 1028–1032. <https://doi.org/10.1130/g47647.1>
- Edwards, M. A., Jackson, M. G., Kylander-Clark, A. R. C., Harvey, J., Hagen-Peter, G. A., Seward, G. G. E., et al. (2019). Extreme enriched and heterogeneous <sup>87</sup>Sr/<sup>86</sup>Sr ratios recorded in magmatic plagioclase from the Samoan hotspot. *Earth and Planetary Science Letters*, *511*, 190–201. <https://doi.org/10.1016/j.epsl.2019.01.040>
- Elliott, T., Plank, T., Zindler, A., White, W., & Bourdon, B. (1997). Element transport from slab to volcanic front at the Mariana arc. *Journal of Geophysical Research*, *102*(B7), 14991–15019. <https://doi.org/10.1029/97jb00788>
- Evans, K. A., Elburg, M. A., & Kamenetsky, V. S. (2012). Oxidation state of subarc mantle. *Geology*, *40*(9), 783–786. <https://doi.org/10.1130/g33037.1>
- Fang, S.-B., Huang, J., Zhang, X.-C., Ionov, D. A., Zhao, Z.-F., & Huang, F. (2022). Zinc isotope fractionation in mantle rocks and minerals, and a revised  $\delta^{66}\text{Zn}$  value for the Bulk Silicate Earth. *Geochimica et Cosmochimica Acta*, *338*, 79–92. <https://doi.org/10.1016/j.gca.2022.10.017>
- Fitzpayne, A., Giuliani, A., Hergt, J., Phillips, D., & Janney, P. (2018). New geochemical constraints on the origins of MARID and PIC rocks: Implications for mantle metasomatism and mantle-derived potassic magmatism. *Lithos*, *318*–319, 478–493. <https://doi.org/10.1016/j.lithos.2018.08.036>
- Fitzpayne, A., Giuliani, A., Maas, R., Hergt, J., Janney, P., & Phillips, D. (2019). Progressive metasomatism of the mantle by kimberlite melts: Sr–Nd–Hf–Pb isotope compositions of MARID and PIC minerals. *Earth and Planetary Science Letters*, *509*, 15–26. <https://doi.org/10.1016/j.epsl.2018.12.013>
- Foden, J., Sossi, P. A., & Nebel, O. (2018). Controls on the iron isotopic composition of global arc magmas. *Earth and Planetary Science Letters*, *494*, 190–201. <https://doi.org/10.1016/j.epsl.2018.04.039>
- Grimes, C. B., John, B. E., Kelemen, P. B., Mazdab, F. K., Wooden, J. L., Cheadle, M. J., et al. (2007). Trace element chemistry of zircons from oceanic crust: A method for distinguishing detrital zircon provenance. *Geology*, *35*(7), 643–646. <https://doi.org/10.1130/g23603a.1>
- Hauff, F., Hoernle, K., & Schmidt, A. (2003). Sr–Nd–Pb composition of Mesozoic Pacific oceanic crust (Site 1149 and 801, ODP Leg 185): Implications for alteration of ocean crust and the input into the Izu-Bonin-Mariana subduction system. *Geochemistry, Geophysics, Geosystems*, *4*(8), 8913. <https://doi.org/10.1029/2002gc000421>
- Hauri, E. H., Wagner, T. P., & Grove, T. L. (1994). Experimental and natural partitioning of Th, U, Pb and other trace elements between garnet, clinopyroxene and basaltic melts. *Chemical Geology*, *117*(1–4), 149–166. [https://doi.org/10.1016/0009-2541\(94\)90126-0](https://doi.org/10.1016/0009-2541(94)90126-0)
- Hawkesworth, C., Cawood, P. A., & Dhuime, B. (2020). The evolution of the continental crust and the onset of plate tectonics. *Frontiers of Earth Science*, *8*, 326. <https://doi.org/10.3389/feart.2020.00326>
- He, Y., Ke, S., Teng, F.-Z., Wang, T., Wu, H., Lu, Y., & Li, S. (2015). High-precision iron isotope analysis of geological reference materials by high-resolution MC-ICP-MS. *Geostandards and Geoanalytical Research*, *39*(3), 341–356. <https://doi.org/10.1111/j.1751-908X.2014.00304.x>
- Hermann, J., & Rubatto, D. (2009). Accessory phase control on the trace element signature of sediment melts in subduction zones. *Chemical Geology*, *265*(3–4), 512–526. <https://doi.org/10.1016/j.chemgeo.2009.05.018>
- Hu, J., Jiang, N., Carlson, R. W., Guo, J., Fan, W., Huang, F., et al. (2019). Metasomatism of the crust-mantle boundary by melts derived from subducted sedimentary carbonates and silicates. *Geochimica et Cosmochimica Acta*, *260*, 311–328. <https://doi.org/10.1016/j.gca.2019.06.033>
- Hu, Y., Teng, F.-Z., Zhang, H.-F., Xiao, Y., & Su, B.-X. (2016). Metasomatism-induced mantle magnesium isotopic heterogeneity: Evidence from pyroxenites. *Geochimica et Cosmochimica Acta*, *185*, 88–111. <https://doi.org/10.1016/j.gca.2015.11.001>
- Huang, J., Ackerman, L., Zhang, X. C., & Huang, F. (2019). Mantle Zn isotopic heterogeneity caused by melt-rock reaction: Evidence from Fe-rich peridotites and pyroxenites from the Bohemian Massif, Central Europe. *Journal of Geophysical Research: Solid Earth*, *124*(4), 3588–3604. <https://doi.org/10.1029/2018jb017125>
- Huang, J., Zhang, X.-C., Chen, S., Tang, L., Wörner, G., Yu, H., & Huang, F. (2018). Zinc isotopic systematics of Kamchatka-Aleutian arc magmas controlled by mantle melting. *Geochimica et Cosmochimica Acta*, *238*, 85–101. <https://doi.org/10.1016/j.gca.2018.07.012>
- Jackson, M. G., Hart, S. R., Koppers, A. A., Staudigel, H., Konter, J., Blusztajn, J., et al. (2007). The return of subducted continental crust in Samoan lavas. *Nature*, *448*(7154), 684–687. <https://doi.org/10.1038/nature06048>
- Kessel, R., Schmidt, M. W., Ulmer, P., & Pettko, T. (2005). Trace element signature of subduction-zone fluids, melts and supercritical liquids at 120–180 km depth. *Nature*, *437*(7059), 724–727. <https://doi.org/10.1038/nature03971>
- Kogiso, T., Tatsumi, Y., & Nakano, S. (1997). Trace element transport during dehydration processes in the subducted oceanic crust: I. Experiments and implications for the origin of ocean island basalts. *Earth and Planetary Science Letters*, *148*(1–2), 193–205. [https://doi.org/10.1016/s0012-821x\(97\)00018-6](https://doi.org/10.1016/s0012-821x(97)00018-6)

- Konter, J. G., Pietruszka, A. J., Hanan, B. B., Finlayson, V. A., Craddock, P. R., Jackson, M. G., & Dauphas, N. (2016). Unusual  $\delta$  56 Fe values in Samoan rejuvenated lavas generated in the mantle. *Earth and Planetary Science Letters*, *450*, 221–232. <https://doi.org/10.1016/j.epsl.2016.06.029>
- Lei, Y., Li, M., Wang, Z., Zhu, Y., Hu, Z., Liu, Y., & Chai, X. (2022). Iron isotopic measurement using large-geometry high-resolution multi-collector inductively coupled plasma mass spectrometer. *Atomic Spectroscopy*, *43*(03), 214–222. <https://doi.org/10.46770/as.2022.111>
- Little, S. H., Vance, D., McManus, J., & Severmann, S. (2016). Key role of continental margin sediments in the oceanic mass balance of Zn and Zn isotopes. *Geology*, *44*(3), 207–210. <https://doi.org/10.1130/g37493.1>
- Liu, S.-A., & Li, S.-G. (2019). Tracing the deep carbon cycle using metal stable isotopes: Opportunities and challenges. *Engineering*, *5*(3), 448–457. <https://doi.org/10.1016/j.eng.2019.03.007>
- Liu, S.-A., Qu, Y.-R., Wang, Z.-Z., Li, M.-L., Yang, C., & Li, S.-G. (2022). The fate of subducting carbon tracked by Mg and Zn isotopes: A review and new perspectives. *Earth-Science Reviews*, *228*, 104010. <https://doi.org/10.1016/j.earscirev.2022.104010>
- Liu, S.-A., Wang, Z.-Z., Li, S.-G., Huang, J., & Yang, W. (2016). Zinc isotope evidence for a large-scale carbonated mantle beneath eastern China. *Earth and Planetary Science Letters*, *444*, 169–178. <https://doi.org/10.1016/j.epsl.2016.03.051>
- Liu, S. A., Wang, Z. Z., Yang, C., Li, S. G., & Ke, S. (2020). Mg and Zn isotope evidence for two types of mantle metasomatism and deep recycling of magnesium carbonates. *Journal of Geophysical Research: Solid Earth*, *125*(11), e2020JB020684. <https://doi.org/10.1029/2020jb020684>
- Liu, Y., Gao, S., Hu, Z., Gao, C., Zong, K., & Wang, D. (2010). Continental and oceanic crust recycling-induced melt-peridotite interactions in the Trans-North China Orogen: U-Pb dating, Hf isotopes and trace elements in zircons from mantle xenoliths. *Journal of Petrology*, *51*(1–2), 537–571. <https://doi.org/10.1093/ptrology/egp082>
- Liu, Y., Gao, S., Jin, S., Hu, S., Sun, M., Zhao, Z., & Feng, J. (2001). Geochemistry of lower crustal xenoliths from Neogene Hannuoba basalt, North China craton: Implications for petrogenesis and lower crustal composition. *Geochimica et Cosmochimica Acta*, *65*(15), 2589–2604. [https://doi.org/10.1016/s0016-7037\(01\)00609-3](https://doi.org/10.1016/s0016-7037(01)00609-3)
- Liu, Y., Gao, S., Lee, C.-T. A., Hu, S., Liu, X., & Yuan, H. (2005). Melt–peridotite interactions: Links between garnet pyroxenite and high-Mg# signature of continental crust. *Earth and Planetary Science Letters*, *234*(1–2), 39–57. <https://doi.org/10.1016/j.epsl.2005.02.034>
- McDonough, W. F., & Sun, S. S. (1995). The composition of the Earth. *Chemical Geology*, *120*(3–4), 223–253. [https://doi.org/10.1016/0009-2541\(94\)00140-4](https://doi.org/10.1016/0009-2541(94)00140-4)
- Moynier, F., Vance, D., Fujii, T., & Savage, P. (2017). The isotope geochemistry of zinc and copper. *Reviews in Mineralogy and Geochemistry*, *82*(1), 543–600. <https://doi.org/10.2138/rmg.2017.82.13>
- Mysen, B. O. (1978). Experimental determination of nickel partition coefficients between liquid, pargasite, and garnet peridotite minerals and concentration limits of behavior according to Henry's law at high pressure and temperature. *American Journal of Science*, *278*(2), 217–243. <https://doi.org/10.2475/ajs.278.2.217>
- Nebel, O., Sossi, P. A., Bénard, A., Wille, M., Vroon, P. Z., & Arculus, R. J. (2015). Redox-variability and controls in subduction zones from an iron-isotope perspective. *Earth and Planetary Science Letters*, *432*, 142–151. <https://doi.org/10.1016/j.epsl.2015.09.036>
- O'Reilly, S. Y., & Griffin, W. L. (2013). Mantle metasomatism. In D. E. Harlov & H. Austrheim (Eds.), *Metasomatism and the chemical transformation of rock: The role of fluids in terrestrial and extraterrestrial processes* (pp. 471–533). Springer. [https://doi.org/10.1007/978-3-642-28394-9\\_12](https://doi.org/10.1007/978-3-642-28394-9_12)
- Plank, T., & Langmuir, C. H. (1998). The chemical composition of subducting sediment and its consequences for the crust and mantle. *Chemical Geology*, *145*(3–4), 325–394. [https://doi.org/10.1016/s0009-2541\(97\)00150-2](https://doi.org/10.1016/s0009-2541(97)00150-2)
- Pons, M. L., Debret, B., Bouilhol, P., Delacour, A., & Williams, H. (2016). Zinc isotope evidence for sulfate-rich fluid transfer across subduction zones. *Nature Communications*, *7*(1), 13794. <https://doi.org/10.1038/ncomms13794>
- Qian, S.-P., Ren, Z.-Y., Zhang, L., Hong, L.-B., & Liu, J.-Q. (2015). Chemical and Pb isotope composition of olivine-hosted melt inclusions from the Hannuoba basalts, North China Craton: Implications for petrogenesis and mantle source. *Chemical Geology*, *401*, 111–125. <https://doi.org/10.1016/j.chemgeo.2015.02.018>
- Rudnick, R. L., & Gao, S. (2014). Composition of the continental crust. In H. D. Holland & K. K. Turekian (Eds.), *Treatise on geochemistry* (2nd ed., pp. 1–51). Elsevier. <https://doi.org/10.1016/B978-0-08-095975-7.00301-6>
- Rudnick, R. L., Gao, S., Ling, W. L., Liu, Y. S., & McDonough, W. F. (2004). Petrology and geochemistry of spinel peridotite xenoliths from Hannuoba and Qixia, North China craton. *Lithos*, *77*(1–4), 609–637. <https://doi.org/10.1016/j.lithos.2004.03.033>
- Salters, V. J. M., & Stracke, A. (2004). Composition of the depleted mantle. *Geochemistry, Geophysics, Geosystems*, *5*(5), Q05B07. <https://doi.org/10.1029/2003GC000597>
- Schiano, P., Clocchiatti, R., Shimizu, N., Maury, R. C., Jochum, K. P., & Hofmann, A. W. (1995). Hydrous, silica-rich melts in the sub-arc mantle and their relationship with erupted arc lavas. *Nature*, *377*(6550), 595–600. <https://doi.org/10.1038/377595a0>
- Schmidberger, S. S., Simonetti, A., & Francis, D. (2003). Small-scale Sr isotope investigation of clinopyroxenes from peridotite xenoliths by laser ablation MC-ICP-MS—Implications for mantle metasomatism. *Chemical Geology*, *199*(3–4), 317–329. [https://doi.org/10.1016/s0009-2541\(03\)00125-6](https://doi.org/10.1016/s0009-2541(03)00125-6)
- Shu, Z. T., Liu, S. A., Prelević, D., Wang, Y., Foley, S. F., Cvetković, V., & Li, S. (2023). Recycled carbonate-bearing silicate sediments in the sources of circum-Mediterranean K-rich lavas: Evidence from Mg-Zn isotopic decoupling. *Journal of Geophysical Research: Solid Earth*, *128*(3), e2022JB025135. <https://doi.org/10.1029/2022jb025135>
- Smart, K. A., Tappe, S., Ishikawa, A., Pfänder, J. A., & Stracke, A. (2019). K-rich hydrous mantle lithosphere beneath the Ontong Java Plateau: Significance for the genesis of oceanic basalts and Archean continents. *Geochimica et Cosmochimica Acta*, *248*, 311–342. <https://doi.org/10.1016/j.gca.2019.01.013>
- Sossi, P. A., Halverson, G. P., Nebel, O., & Eggins, S. M. (2015). Combined separation of Cu, Fe and Zn from rock matrices and improved analytical protocols for stable isotope determination. *Geostandards and Geoanalytical Research*, *39*(2), 129–149. <https://doi.org/10.1111/j.1751-908X.2014.00298.x>
- Sossi, P. A., Nebel, O., & Foden, J. (2016). Iron isotope systematics in planetary reservoirs. *Earth and Planetary Science Letters*, *452*, 295–308. <https://doi.org/10.1016/j.epsl.2016.07.032>
- Sossi, P. A., Nebel, O., O'Neill, H. S. C., & Moynier, F. (2018). Zinc isotope composition of the Earth and its behaviour during planetary accretion. *Chemical Geology*, *477*, 73–84. <https://doi.org/10.1016/j.chemgeo.2017.12.006>
- Stepanov, A. S., & Hermann, J. (2013). Fractionation of Nb and Ta by biotite and phengite: Implications for the “missing Nb paradox”. *Geology*, *41*(3), 303–306. <https://doi.org/10.1130/g33781.1>
- Straub, S. M., Gómez-Tuena, A., & Vannucchi, P. (2020). Subduction erosion and arc volcanism. *Nature Reviews Earth & Environment*, *1*(11), 574–589. <https://doi.org/10.1038/s43017-020-0095-1>
- Tatsumoto, M., Basu, A. R., Wankang, H., Junwen, W., & Guanghong, X. (1992). Sr, Nd, and Pb isotopes of ultramafic xenoliths in volcanic rocks of Eastern China: Enriched components EMI and EMII in subcontinental lithosphere. *Earth and Planetary Science Letters*, *113*(1–2), 107–128. [https://doi.org/10.1016/0012-821x\(92\)90214-g](https://doi.org/10.1016/0012-821x(92)90214-g)

- Teng, F.-Z., Dauphas, N., Huang, S., & Marty, B. (2013). Iron isotopic systematics of oceanic basalts. *Geochimica et Cosmochimica Acta*, 107, 12–26. <https://doi.org/10.1016/j.gca.2012.12.027>
- Wang, Z.-Z., Liu, S.-A., Liu, J., Huang, J., Xiao, Y., Chu, Z.-Y., et al. (2017). Zinc isotope fractionation during mantle melting and constraints on the Zn isotope composition of Earth's upper mantle. *Geochimica et Cosmochimica Acta*, 198, 151–167. <https://doi.org/10.1016/j.gca.2016.11.014>
- Williams, H. M., & Bizimis, M. (2014). Iron isotope tracing of mantle heterogeneity within the source regions of oceanic basalts. *Earth and Planetary Science Letters*, 404, 396–407. <https://doi.org/10.1016/j.epsl.2014.07.033>
- Wu, F.-Y., Yang, J.-H., Xu, Y.-G., Wilde, S. A., & Walker, R. J. (2019). Destruction of the North China craton in the Mesozoic. *Annual Review of Earth and Planetary Sciences*, 47(1), 173–195. <https://doi.org/10.1146/annurev-earth-053018-060342>
- Xu, R., Liu, Y., Lambert, S., Hoernle, K., Zhu, Y., Zou, Z., et al. (2022). Decoupled Zn-Sr-Nd isotopic composition of continental intraplate basalts caused by two-stage melting process. *Geochimica et Cosmochimica Acta*, 326, 234–252. <https://doi.org/10.1016/j.gca.2022.03.014>
- Xu, R., Liu, Y., Tong, X., Hu, Z., Zong, K., & Gao, S. (2013). In-situ trace elements and Li and Sr isotopes in peridotite xenoliths from Kuan-dian, North China Craton: Insights into Pacific slab subduction-related mantle modification. *Chemical Geology*, 354, 107–123. <https://doi.org/10.1016/j.chemgeo.2013.06.022>
- Xu, Y. (2002). Evidence for crustal components in the mantle and constraints on crustal recycling mechanisms: Pyroxenite xenoliths from Hannuoba, North China. *Chemical Geology*, 182(2–4), 301–322. [https://doi.org/10.1016/s0009-2541\(01\)00300-x](https://doi.org/10.1016/s0009-2541(01)00300-x)
- Yang, C., & Liu, S. A. (2019). Zinc isotope constraints on recycled oceanic crust in the mantle sources of the Emeishan large igneous province. *Journal of Geophysical Research: Solid Earth*, 124(12), 12537–12555. <https://doi.org/10.1029/2019jb017405>
- Zhang, G., Liu, Y., Moynier, F., Hu, Z., Zhu, Y., Jiang, X., & Li, M. (2022). Copper mobilization in the lower continental crust beneath cratonic margins, a Cu isotope perspective. *Geochimica et Cosmochimica Acta*, 322, 43–57. <https://doi.org/10.1016/j.gca.2022.01.031>
- Zhang, G., Liu, Y., Moynier, F., Zhu, Y., Wang, Z., Hu, Z., et al. (2020). Zinc isotopic composition of the lower continental crust estimated from lower crustal xenoliths and granulite terrains. *Geochimica et Cosmochimica Acta*, 276, 92–108. <https://doi.org/10.1016/j.gca.2020.02.030>
- Zhang, S.-H., Zhao, Y., Song, B., Hu, J.-M., Liu, S.-W., Yang, Y.-H., et al. (2009). Contrasting Late Carboniferous and Late Permian–Middle Triassic intrusive suites from the northern margin of the North China craton: Geochronology, petrogenesis, and tectonic implications. *Geological Society of America Bulletin*, 121(1–2), 181–200. <https://doi.org/10.1130/b26157.1>
- Zhao, G., Wilde, S. A., Cawood, P. A., & Sun, M. (2001). Archean blocks and their boundaries in the North China Craton: Lithological, geochemical, structural and P–T path constraints and tectonic evolution. *Precambrian Research*, 107(1–2), 45–73. [https://doi.org/10.1016/s0301-9268\(00\)00154-6](https://doi.org/10.1016/s0301-9268(00)00154-6)
- Zhao, X., Cao, H., Mi, X., Evans, N., Qi, Y., Huang, F., & Zhang, H. (2017). Combined iron and magnesium isotope geochemistry of pyroxenite xenoliths from Hannuoba, North China Craton: Implications for mantle metasomatism. *Contributions to Mineralogy and Petrology*, 172(6), 40. <https://doi.org/10.1007/s00410-017-1356-y>
- Zheng, J. P., Griffin, W. L., Qi, L., O'Reilly, S. Y., Sun, M., Zheng, S., et al. (2009). Age and composition of granulite and pyroxenite xenoliths in Hannuoba basalts reflect Paleogene underplating beneath the North China Craton. *Chemical Geology*, 264(1–4), 266–280. <https://doi.org/10.1016/j.chemgeo.2009.03.011>
- Zhi, X., Song, Y., Frey, F. A., Feng, J., & Zhai, M. (1990). Geochemistry of Hannuoba basalts, eastern China: Constraints on the origin of continental alkalic and tholeiitic basalt. *Chemical Geology*, 88(1–2), 1–33. [https://doi.org/10.1016/0009-2541\(90\)90101-c](https://doi.org/10.1016/0009-2541(90)90101-c)
- Zhu, Y., Li, M., Wang, Z., Zou, Z., Hu, Z., Liu, Y., et al. (2019). High-precision copper and zinc isotopic measurements in igneous rock standards using large-geometry MC-ICP-MS. *Atomic Spectroscopy*, 40(6), 206–214. <https://doi.org/10.46770/AS.2019.06.002>
- Zong, K., Liu, Y., Gao, S., Yuan, H., Liu, X., & Wang, X. (2005). In situ trace elemental compositions and geodynamic significance of clinopyroxene in pyroxenite xenoliths from Hannuoba. *Acta Petrologica Sinica*, 21(3), 909–920. <https://doi.org/10.3969/j.issn.1000-0569.2005.03.029>
- Zou, D., Liu, Y., Hu, Z., Gao, S., Zong, K., Xu, R., et al. (2014). Pyroxenite and peridotite xenoliths from Hexigten, Inner Mongolia: Insights into the Paleo-Asian Ocean subduction-related melt/fluid–peridotite interaction. *Geochimica et Cosmochimica Acta*, 140, 435–454. <https://doi.org/10.1016/j.gca.2014.05.046>

## References From the Supporting Information

- Dai, W., Wang, Z., Liu, Y., Chen, C., Zong, K., Zhou, L., et al. (2020). Calcium isotope compositions of mantle pyroxenites. *Geochimica et Cosmochimica Acta*, 270, 144–159. <https://doi.org/10.1016/j.gca.2019.11.024>
- Gao, S., Rudnick, R. L., Yuan, H. L., Liu, X. M., Liu, Y. S., Xu, W. L., et al. (2004). Recycling lower continental crust in the North China craton. *Nature*, 432(7019), 892–897. <https://doi.org/10.1038/nature03162>
- Liu, Y., Hu, Z., Gao, S., Guenther, D., Xu, J., Gao, C., & Chen, H. (2008a). In situ analysis of major and trace elements of anhydrous minerals by LA-ICP-MS without applying an internal standard. *Chemical Geology*, 257(1–2), 34–43. <https://doi.org/10.1016/j.chemgeo.2008.08.004>
- Liu, Y., Zong, K., Kelemen, P. B., & Gao, S. (2008b). Geochemistry and magmatic history of eclogites and ultramafic rocks from the Chinese continental scientific drill hole: Subduction and ultrahigh-pressure metamorphism of lower crustal cumulates. *Chemical Geology*, 247(1–2), 133–153. <https://doi.org/10.1016/j.chemgeo.2007.10.016>
- Tong, X., Liu, Y., Hu, Z., Chen, H., Zhou, L., Hu, Q., et al. (2016). Accurate determination of Sr isotopic compositions in clinopyroxene and silicate glasses by LA-MC-ICP-MS. *Geostandards and Geoanalytical Research*, 40(1), 85–99. <https://doi.org/10.1111/j.1751-908X.2015.00315.x>